Master's Thesis

Evaluating load-balancing potential for the energy system provided through distribution grid flexibilities

presented by:

Julian Endres

student number: 353273

Primary Reviewer:	Prof. Dr. Tom Brown, TU Berlin
Supervisor TU Berlin:	Dr.-Ing. Fabian Neumann, TU Berlin
Supervisor RLI:	M.Sc. Birgit Schachler, Reiner Lemoine Institut
	M.Sc. Anya Heider, Reiner Lemoine Institut
submitted:	April 10, 2023

Technical University of Berlin
Department of Digital Transformation in Energy Systems
Institut of Energy Engineering

Eidesstattliche Erklärung

Hiermit erkläre ich, dass ich die vorliegende Arbeit selbstständig und eigenhändig sowie ohne unerlaubte fremde Hilfe und ausschließlich unter Verwendung der aufgeführten Quellen und Hilfsmittel angefertigt habe.

Berlin, 10. April 2023

Julian Endres

Acknowledgment

I would like to express my sincere gratitude to my colleagues at the RLI for their invaluable contribution to this research. Their advice, contribution to the input data and tools used were essential to the success of this project, and I am deeply grateful for their support.

Thank you to everyone who contributed to the success of this project.

Abstract

In this study, we determined the minimum required reinforcement and flexibility potential of six distribution networks using flexible demand components such as heat pump (HP) and battery electric vehicle (BEV) and additional network reinforcement. renewable energy sources (RES) capacities and a penetration of flexible demand units for a projected horizon of 2035 were applied to synthetic distribution grid networks. The methodology involves identifying specific observation periods based on the residual load, optimizing the minimal line loading dispatch of flexible components, and deriving a minimal required reinforcement. Based on the minimal reinforcement scenario, five scenarios with additional reinforcement are defined to evaluate the increasing flexibility potential that all aggregated components could provide to the overlying network. Finally, the study deduced the flexibility of all aggregated HPs and BEVs using flex-bands and the defined metric load balancing potential to provide insight into the ability of the distribution system to support the overlying transmission system.

Zusammenfassung

In dieser Studie haben wir den minimal erforderlichen Netzausbau und das Flexibilitätspotenzial von sechs Verteilungsnetzen unter Verwendung flexibler Lastkompenten wie Wärmepumpe und Elektroautos sowie zusätzlichen Netzausbau ermittelt. RES-Kapazitäten und eine Durchdringung mit flexiblen Lasten für einen Prognosehorizont von 2035 wurden auf synthetische Verteilnetze angewendet. Die Methodik umfasst die Identifizierung spezifischer Beobachtungszeiträume auf der Grundlage der Residuallast, die Optimierung der minimalen Leitungsauslastung flexibler Komponenten und die Ableitung einer minimal erforderlichen Netzverstärkung. Basierend auf dem Szenario des minimalen Netzausbaus werden fünf Szenarien mit zusätzlicher Verstärkung definiert, um das zunehmende Flexibilitätspotenzial zu bewerten, das alle aggregierten Komponenten dem übergeordneten Netz bieten könnten. Schließlich wurde in der Studie die Flexibilität aller aggregierten Wärmepumpen und Elektroautos unter Verwendung von Flexibilitätsbändern und der definierten Metrik 'Lastausgleichspotential' abgeleitet, um einen Einblick in die Fähigkeit des Verteilnetztes zu geben, das übergeordnete Übertragungsnetz zu unterstützen.

Contents

Glossary

($\mathcal{N}-1$) '(N-1) criterion' means the rule according to which the elements remaining in operation within a TSO's control area after occurrence of a contingency are capable of accommodating the new operational situation without violating operational security limits [1].

`demandlib` A tool which creates scale standard heat and power demand profiles with annual values. GitHub

`ding0` A tool to generate synthetic medium and low voltage (LV) power distribution grid (DG) based on open accessible data. GitHub

`eDisGo` A framework to evaluate flexibility measures as an economic alternative to conventional grid expansion in medium and low voltage grids. GitHub

`eGon-data` Part of the eGo^n project which deals with the importing, generating and processing of the data used. GitHub

`feedinlib` A tool to connect weather data interfaces with interfaces of wind and pv power models. GitHub

`Pyomo` a Python library for modeling optimization problems.Website

`PyPSA` PyPSA is an open source toolbox for simulating and optimising modern power and energy systems. Read the docs

`SimBEV` A tool for the simulation of electric vehicle charging demand.GitHub

`TracBEV` A tool for the regional allocation of charging infrastructure. Using results from `SimBEV` to place the corresponding charging points on a map. GitHub

battery electric vehicle In this work we refer to both battery electric vehicle (BEV) and plug-in hybrid electric vehicle (PHEV).

feed-in management Decreasing the feed-in of electricity from variable renewable energy sources (vRES) in case of congestions.

flex-band A flex-band, or flexibility band is a concept, which describes an interval or specific range in which flexible appliances operate. The band is bounded by an upper and lower bound. The concept is further described in Section 2.2.5.

new consumers Electrical devices that are integrated into the energy system as part of sector coupling (here: heat pump (HP), battery electric vehicle (BEV)).

Open-Energy-Platform The Open-Energy-Platform (OEP) is a portal for modelers who want to create a more open, transparent research landscape in energy systems analysis. It provides tools that allow to search and visualize the OEDB data. Website

redispatch Intervention upon request of transmission system operator (TSO) or distribution system operator (DSO) to adjust the feed-in upstream and downstream of a regional overload.

residual load The difference between electricity demand and supply from variable renewable energy sources.

Acronyms

AC-OPF	alternating current optimal power flow
BESS	battery energy storage system
BEV	battery electric vehicle
BFM	branch flow model
BIM	bus injection model
COP	coefficient of performance
CP	charging park
DER	distributed energy resources
DG	distribution grid
DR	demand response
dRES	dispatchable renewable energy sources
DSM	demand side management
DSO	distribution system operator
EHV	extra high voltage
FIM	feed-in management
GW	gigawatt
HP	heat pump
HPC	high power charging
HV	high voltage
LBP	load balancing potential
LV	low voltage
MV	medium voltage
MVGD	medium voltage grid district
MW	megawatt
NDP	German network development plan
OEP	Open-Energy-Platform
OPF	optimal power flow
OSM	OpenStreetMap
PHEV	plug-in hybrid electric vehicle
PP	power plant
PV	photovoltaic
RES	renewable energy sources
SOC	state of charge
SOE	state of energy
TES	thermal energy storage
TG	transmission grid
TSO	transmission system operator
vRES	variable renewable energy sources

List of Symbols

Angles

ϕ	Complex current phasor angle
ψ	Complex quantity angle
θ	Complex voltage phasor angle

Notation

$\boldsymbol{k}$	Constant k
ω_t	Length of Time Step t
j	Imaginary Unit
K	Parameter k
k	Variable k
k^*	Complex Conjugate
k^{el}	Electrical
k^{EV}	Electric Vehicle
k^{HP}	Heat Pump
k^{th}	Thermal
k_i	Index i
k_t	Time Step t

Physical Quantities

$\cdot Q$	Heat demand
η	Efficiency
B	Susceptance
G	Conductance
I	Current
P	Real Power
Q	Reactive Power
S	Apparent Power
V	Voltage
X^d	Demand
X^g	Generation
Y	Admittance
Z	Impedance
SOC	State of Charge
SOE	State of Energy

Sets

B	Branches, ”Network Edges”
CP	Charging Points
HP	Heat Pumps
N	Buses, ”Network Nodes”
T	Time Steps

List of Figures

List of Tables

1 Introduction

In the past, megawatt (MW) to gigawatt (GW) power plants (PPs) were used to generate electricity outside the load centers, connected to the high voltage (HV) and extra high voltage (EHV) level. The electricity was transported unidirectionally to the centers and distributed via medium voltage (MV) and low voltage (LV) grids. However, the energy transition in Germany is leading to an increasing share of distributed energy resources (DER), which are predominantly integrated into the distribution grid (DG) (approx. 96% in 2015[2]), due to their low generation capacities. Thus, the simultaneous occurrence of peak load [3] and high feed-in from variable renewable energy sources (vRES) can lead to line and transformer overloads caused by changing load flow situations. Measures like, feed-in management (FIM) or redispatch are currently the only methods to resolve congestion's. To prevent these and to avoid excessive curtailment of variable renewable energy sources (vRES), grid expansion will be necessary but this requires long-term investments and planning. Furthermore, it is still unclear how exactly generation and consumption will develop in the distribution grids (DGs). In the course of sector coupling, new consumers such as battery electric vehicle (BEV) and heat pump (HP) will additionally lead to higher demands. Without coordination mechanisms, peak demand may be disproportionately higher than total energy consumption. DG bottlenecks will therefore occur more frequently in the future and need to be addressed with new approaches. If coordinated, battery electric vehicles (BEVs) and heat pumps (HPs) with thermal energy storage (TES) can provide temporal flexibility and can be used as an alternative to FIM to reduce peak demand and help to avoid or limit the necessary grid expansion. How to coordinate and make the potential of flexibility options accessible to grid operators is still up for discussion [2] but they could be activated at short notice to ensure a functioning grid. Quantifying the potential and effectiveness of flexibility by new consumers is the focus of current research. This is necessary to understand the effects and to support the decision making process to set the right regulatory framework [4]. This work aims to contribute to that process.

1.1 Context

The thesis is based on the research project *eGon* at the Reiner-Lemoine-Institute, which examines the impact of sector coupling on the power grid [5]. The project aims to improve the planning tool *eGo*, which is used to identify cost-effective grid expansion scenarios [6].

One of the components is `eDisGo`[7], a program developed for optimizing grid expansion and storage positioning. The current research project focuses on incorporating BEVs, HPs with TES, battery energy storage system (BESS) and demand side management (DSM) as sources of flexibility to reduce the costs of expanding the grid.

1.2 Scope

In this work, we determine a minimum grid expansion necessary to integrate the additional loads that will be added as part of sector coupling. For this purpose, we consider the optimal deployment of HP and BEV. Based on the minimum grid expansion, we want to investigate to what extent additional grid expansion makes it possible to use free capacities in order to pass them on to the transmission grid. The so-called load balancing potential (LBP) is used to evaluate the interplay of temporal (BEV and HP with TES) and spatial (grid reinforcement) flexibility. Therefore we want to answer the following questions:

- What is the minimum required grid expansion in DGs using all flexibility options (BEVs and HPs)?
- Which load balancing potential can be provided to the overlying grid levels using all flexibility options and considering the minimum required grid expansion?
- How does the provided load balancing potential increase with increasing grid expansion?

1.3 Structure

This work is structured as follows: first, in Chapter 2, an overview of German power system and network modeling techniques is given, as well as a comparative analysis of current research. Then, in Chapter 3, we describe the data and tools that form the basis of the research. Next, the methodology for assessing flexibility potential in Chapter 4 is described and justified. This is followed by the presentation, explanation, and discussion of the results in Chapter 5. Finally, Chapter 6 summarizes the work and provides an outlook for further research.

2 Related Work

An overview of the German power system and modeling techniques is presented in this chapter to provide context for the work at hand. First, the description of the underlying grid structure is given (Section 2.1.1), followed by pointing out the challenges of the system in transition. The particular challenges of sector coupling are then examined (Section 2.1.3). Applications and measures used to address these challenges and lift potentials in the power system are introduced in Section 2.1.4.

Fundamentals of modeling power networks are introduced in the next section (Section 2.2), including a description of power flow analysis methods in Section 2.2.1. A basic optimal power flow model is then demonstrated in Section 2.2.2, building on the previously derived functions and presenting the relaxation used in this work. Curtailment and the reinforcement strategies implemented in `eDisGo` are explained in Section 2.2.3 and Section 2.2.4, respectively. In addition, an approach for analyzing the flexibility potential is presented in Section 2.2.5. Finally, the current research focus and the questions that our work aims to cover are discussed in Section 2.3.

2.1 Power System

The power system in Germany is a complex interplay between the energy market and the physical grid. While the energy market neglects the constraints of the physical grid, such as congestions, and assumes a ”copperplate” without barriers, it operates grid-independently following the merit-order system. This system determines the most cost-effective way to dispatch electricity generation sources, with the cheapest sources being dispatched first, and promotes the adoption of renewable energy sources. The market aims to organize a balanced total of generation and demand, which historically was achieved by a few dispatchable power plant (PP) that followed predictions with standard load profiles, and hydro pump storage units that were used as flexibility to adjust to unexpected changes. Consequently, power plant dispatch was purely demand-oriented.

However, any inadequacies between the market results and the capacity of the network infrastructure must be addressed shortly before delivery to prevent compromising its stability. Therefore, transmission system operators (TSOs) and distribution system operators (DSOs) need to subsequently control the transmission and distribution of electricity within the physical

boundaries of the grid. This control is essential to ensure the stability of the grid and to avoid overloading, congestion, or even blackouts. It requires a complex interplay of market mechanisms and physical grid operations to maintain a stable and secure power supply.

2.1.1 Grid structure

The transmission network was designed to transport electricity over long distances at high voltages from megawatt (MW) to gigawatt (GW) dispatchable PPs to load centers. Whereas distribution networks were responsible for regional fine distribution at lower voltages. These networks are further classified into extra high voltage (EHV), high voltage (HV), medium voltage (MV), and low voltage (LV) levels, with this work focusing exclusively on the effects on the distribution networks at the MV, and LV levels. To provide clarity, Table 2.1 shows the typical voltages for each level in Germany [8] and their total line length.

Table 2.1: Voltage levels in Germany *DIN VDE 0175*[9] with total line length [10].

Name	**Short**	**V**	**Length**
Extra high voltage	EHV	$\geq$ 220 kV	36.000 km
High voltage	HV	110 kV	96.000 km
Medium voltage	MV	10/20 kV	520.000 km
Low voltage	LV	400 V	1.120.000 km

Historically, the distribution grid (DG) was planned unidirectional, transporting electricity from high to low voltage. For coarse distribution, power is brought to regional substations via 100 kV lines. From here, the primary distribution takes place. Depending on load density or landscape conditions, the nominal voltage (20 kV or 10 kV) and type (overhead line or underground cable) vary. According to DIN 1998, network operators are encouraged to lay power cables in public ground [11]. In urban areas, underground cables with 10 kV are usually used and laied under the streets [12, p.85]. In rural areas, the ratio between 20 kV overhead lines and underground cables is approximately equal. Secondary distribution takes place in the low-voltage level, where underground cables are predominantly used [13].

A basic principle within network planning is the design of the equipment, in a way that the conditions for continuous thermal load and voltage stability are met. This is usually checked by means of load flow calculations (further described in Section 2.2.1). The voltage V of a given network needs to remain within a defined tolerance, also called a voltage band. The corresponding requirements for voltage stability can be found in *EN 50160* [9]. Also, thermal limits must be respected, resulting into a maximum load in operation.

To ensure an uninterrupted power supply, power grids in the MV level are therefore designed according to the $(N-1)$ failure criterion. If a fault or failure occurs within a network, it must be possible to compensate for this fault either structurally or by means of a technical measure. MV grids are usually designed as ring grids with a switch disconnector and operated

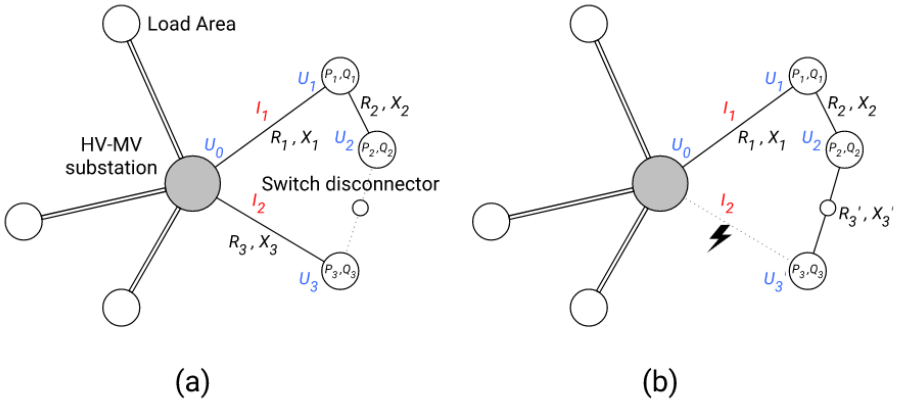

Figure 2.1: Mode of operation in case of a) normal, b) failure in one half ring.

openly. The faulty segment can then be isolated as illustrated in Figure 2.1. The rule does not apply for LV grids, as the $(\mathcal{N}-1)$ criterion is not mandatory at this level. Today, low-voltage networks are largely operated as beam networks due to the simple and clear operating mode [13, p.566].

2.1.2 System in Transformation

In recent years, Germany has made significant progress in expanding its renewable energy capacity, with wind and solar power accounting for 42.8% of the country's electricity generation in 2021 [14]. However, this expansion has also exposed a bottleneck in the country's grid infrastructure. Renewable energy from the north can not be transported to the south in the amount it's generated and allocated by the market. *Redispatch* is used to dissolve the misalignment of market and grid. This program enables grid operators to direct renewable energy producers to decrease their output (feed-in management) during periods of congestion and allocate dispatchable feed-in sources closer to areas of demand. This measure has existed before but was not used to this extent and already causes increasingly high costs just by decreasing renewable energy sources (RES) power as seen in Figure 2.2.

The majority of feed-in management events occur in the DG (67% in 2020), where variable renewable energy sources (vRES) are mostly integrated, although the congestion causing the feed-in management event was located in the transmission grid (TG) in 79% of cases. About 81% of feed-in management events take place in the states of "Schleswig-Holstein" and "Niedersachsen", which have favorable wind conditions and high installed capacity of wind turbines [15, p. 161f]. This is caused particularly because of the transmission of power to the southwest, which has traditionally relied on a combination of fossil fuel-fired power plants and nuclear power [16]. To mitigate the misalignment between renewable energy expansion and demand in the future, intensive grid expansion is needed.

The current need for grid expansion is particularly high in the transmission networks due to

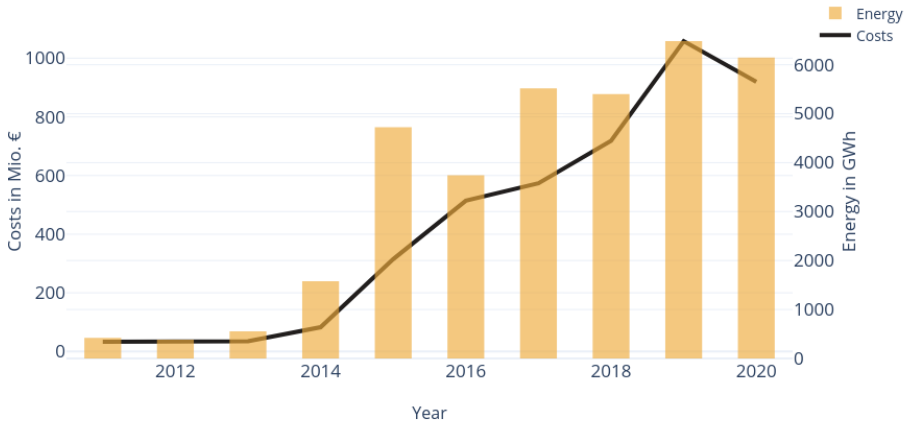

Figure 2.2: Costs and amount of feed-in management in Germany 2011-2020 [15].

the need for redispatch, which is necessary to prevent grid instability caused by inadequacies between the market results and the capacity of the network infrastructure. Historically, distribution networks have been planned with certain margins, but in some cases, these margins are already being stretched to their limits. This situation will intensify with increasing integration of vRES. Over 90% of already installed vRES feeds directly into the LV grid [13, p. 572]. As photovoltaic (PV) capacity increases in the LV level, reverse flows are happening [18] as shown in Figure 2.3. The PV feed-in exceeds the local load and therefore feeds into the higher MV grid. Additionally, the long low voltage feeders in rural networks cause voltage levels to exceed maximum voltage limits [11], [13, p.546]. As a result, there are unacceptable voltage increases and thermal overload of lines and transformers. This situation raises the necessity for reinforcements and to carry out power flow calculations in the DGs as well, whereas traditionally, these calculations were only required in TGs [13, p.567].

2.1.3 Sector Coupling

To address the urgent challenge of climate change and its impacts, we must fundamentally transform how we produce and consume energy. Decarbonizing the electricity system is key to achieving this goal, and requires an integrated and optimized energy system based on electricity. Sector coupling refers to the integration of different energy sectors, including industrial processes, heating, and transportation, into a more unified electricity system with bidirectional flows between all voltage levels, as illustrated in Figure 2.3. This integration involves various technologies and processes that allow for the exchange of different forms of energy, resulting in an increased demand for electricity as more sectors transition to using renewable energy sources (RES).

It's worth noting that with the increasing share of renewable energy sources, generation and demand peaks occur much more frequently in shorter timeframes than in the previous load-

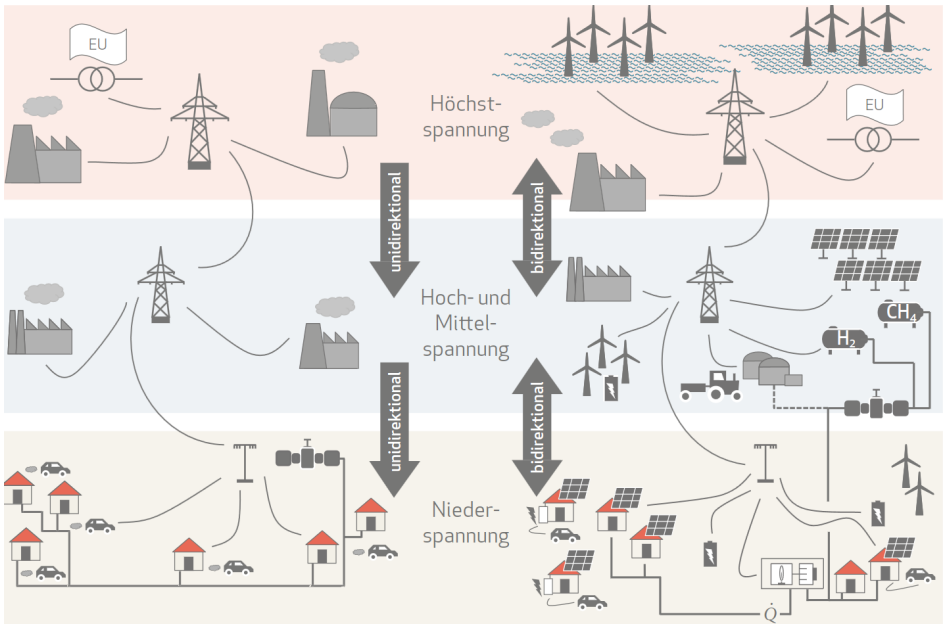

Figure 2.3: Comparison of the traditional (left) and future energy system (right) [17]

dominated system. This presents challenges for the electricity grid, as traditional supply-side measures may not be sufficient to ensure stability and reliability.

Currently, curtailment with feed-in management (FIM) or redispatch is the only method available to solve this issue. However, sector coupling can play an essential role in addressing this challenge. By integrating vRES into the grid and storing excess energy for later use in car batteries, thermal storage, or hydrogen production, sector coupling can help to balance supply and demand and avoid grid congestion [17].

At the same time, with further power demand increases, it becomes necessary to expand grid capacity to accommodate the additional load. However, expanding the grid to its full capacity is not cost-efficient, as the simultaneous fluctuations in vRES and power demand for charging electric vehicles and heat pumps can disproportionately increase the line load compared to the average load [4].

Another possibility is demand response (DR) which refers to the practice of adjusting energy consumption patterns in response to changes in the supply. This, and distributed storage capacities, give consumers the possibility to actively take part in the market and become prosumers. DR strategies, such as load shifting, can play an important role in balancing supply and demand and avoiding grid congestion. Moreover, DR can become more cost-effective than grid expansion, once a certain point of penetration is reached [4].

Implementing these technologies into the grid, will foremost require further reinforcement in the DG. If coordinated, their use can provide temporal flexibility and alternatively be used to FIM, reduce peak demand and help to avoid or limit the necessary amount of more reinforcement. Up to now, drivers of sector coupling are mainly heat pumps (Power-to-Heat)

and electric vehicles (Power-to-Mobility) which are both primarily connected to the DG and therefore main components in this work.

2.1.4 Flexibility Options

Flexibility options are an "Asset or measure supporting the power system to balance electric demand and supply and compensate for their stochastic fluctuations stemming from, e.g. weather or consumer behavior." [19]. Therefore, they are an important consideration in the design and operation of DGs, as it allows the grid to respond to fluctuations in demand or supply and hence support the integration of vRES. There are many technologies as already mentioned in Section 2.1.3.

Spatial or network-side flexibility in the electricity grid refers to the ability of the grid to adjust to changes in the demand for electricity across different geographical locations. This is provided by the grid itself and defined by the load capacities of the transformers and lines, allowing the electricity to flow from areas of excess supply to areas of high demand. Grid reinforcement is the process of upgrading and strengthening the existing power grid infrastructure. This involves mostly upgrading lines, transformers or adding parallel components to improve their capacity and reliability to maintain a balanced and efficient flow of electricity.

Temporal flexibility refers to the ability of the grid to respond to changes in demand and supply over different timescales. In the past, conventional power plants have provided flexibility from the supply-side by adjusting their generation to meet current demand, based on their ramping capabilities. However, in order to decarbonize the energy system, these power plants are no longer viable.

To increase flexibility, alternative options include storage (e.g. pumped hydro storage and large-scale batteries), network upgrades, and demand-side flexibility through controllable loads and energy system integration. While pumped hydro storage is the most common energy storage worldwide, it requires specific geographic features and infrastructure, making it costly and time-consuming. Large-scale batteries are gaining traction but still have high upfront costs. Thus, transmission network interconnection and demand-side flexibility often present more cost-effective alternatives. DR (DR) has been proven effective in reducing peak load and allowing for active participation of the demand side in grid operations, improving efficiency, reliability, and safety.

As a result, hydroelectric power and backup gas power plants are expected to become the main sources of supply-side flexibility going forward, but only in relatively low capacities. While energy storage systems, like pumped hydropower, compressed air storage or battery energy storage system (BESS), may be able to partially cover the supply-side flexibility gap, they will not be able to fully replace the flexibility provided by conventional power plants in the near term. BESS are currently mainly used as home storage in a user-oriented way, maximizing self-consumption of PV power. Like this, they do not cause any additional stress to the grid, but

could even provide ancillary services if a regulatory framework with corresponding incentives would be in place [20].

With DR, consumers reduce their energy use during peak periods or shift their consumption to off-peak hours without changing overall energy demand in this time frame. As consumers actively take part, this needs some kind of coordination like prices signals when energy from vRES is available or grids aren't overloaded. Although, DR might have many benefits, such as preventing grid overloads and thus reducing redispatch costs, various constraints have hindered its adoption. These include the lack of a regulatory framework, reliable prediction tools, and effective communication and control techniques [21][4]. As already mentioned in Section 2.1.3, battery electric vehicles (BEVs) and heat pumps (HPs) are currently the most widespread technologies. Both BEVs and HPs have built-in or usually are built-with storage capacities, making them well-suited for DR. Especially BEVs with its most often long-standing times, offer a lot of temporal flexibility when to be charged, depending on the use cases. Charging at home or at work are assumed to be less time sensitive than public or fast charging. During the standing time, charging can be organized flexible as long as the total amount of energy is met. HP are highly efficient and transform heat from a low-temperature source to an elevated-temperature level, producing three to five times the amount of heat than electricity used. HP themselves are not very flexible in terms of efficiency and load, but complemented with a thermal energy storage (TES), energy losses are traded for a gain in temporal flexibility [22]. Sizing of the HP foremost depends on the heat demand and the size of the TES. HP can be applied in various context and sizes depending on the amount of heat needed. In this work, we solely consider household applications.

It's worth noting that if used in a grid-supportive way, the deployment of flexible appliances like HPs and BEVs can be an advantage for grid operators. These can be used to shift electricity demand from peak periods to off-peak periods. If coordinated, this services can help to stabilize the grid and reduce the need for expensive peaking power plants. This can reduce the need for new infrastructure investments and lower the overall cost of electricity for consumers. However, for many of them, economically viable concepts are only competitive under certain conditions [23]. This needs to be addressed by the regulatory framework. Grid modeling can help to determine the technical aspects, how these devices can be used to support the grid, and what requirements need to be in place. In this work, we focus on the interplay between temporal flexibility from both BEVs and HPs with TES and increasing spatial flexibility from grid reinforcement. We evaluate what amount of reinforcement is needed and how additional grid expansion impacts the potential of flexibility.

2.2 Power Networks Modeling

Modeling power networks serves the purpose of analyzing the network infrastructure. Power flow modeling and optimization techniques are widely used to analyze power grids and to

identify potential expansion scenarios [24], [25]. The flow of electricity through the grid and its behavior can be studied under different operating conditions to identify opportunities to improve its performance and reliability. To ensure continuous operation of the network, network operators must adequately dimension their grids or intervene at short notice as the electricity grid needs to be operated in certain boundaries [12] to ensure the following:

- Frequency stability
- Voltage stability
- No overloads
- Outage backup

In order to estimate the grid load in different load scenarios, power flow simulations are conducted. In the context of the energy transition, these methodologies are becoming increasingly important for DGs. This is because the rapid growth of distributed energy resources is changing the way that electricity is generated and consumed, and it is placing new demands on the DG. As a result, DSO must adapt to these changes and invest in expanding and upgrading the grid to ensure that it can support the growing integration of renewable energy. To find out about the impact of new technologies, the optimal power flow can be used. It computes the optimal dispatch of technologies subject to technical and physical constraints and with the aim of achieving a certain objective e.g. minimal line loading or minimal curtailment. With this information, minimal grid expansion scenarios can be determined and potential savings identified. Power flow modeling and optimization can play a key role in supporting these efforts, by providing information about the capabilities and limitations of the grid and helping to identify the most cost-effective and efficient ways to expand and upgrade the grid.

This work is focused on power grid optimization, therefore we want to introduce into the topic of power flow modeling and how the network state is determined. We will then provide the fundamentals of dispatch optimization and how an optimal, feasible solution can be found. After that, will address the limitations and variants to solve particularly complex problems.

2.2.1 Power Flow Analysis

A power flow analysis determines the values of the state variables, e.g. complex bus voltages, for a given operating state of the system. As noted in [26, Chapter 6], to validate that this state is AC-feasible, all of the following conditions must be satisfied:

- The generators must produce sufficient power to cover loads and transmission losses.
- The generators' limits for real and reactive power production must not be exceeded.
- The bus voltages must be close to their nominal values.

To verify that these conditions are met, it is necessary to calculate the power flow from generators to loads throughout the electrical network. This process is referred to as the *"power flow problem"*. The main components are edges, *"lines"* and nodes, *"buses"*. The buses must be classified into one of the following three categories [27, Page 332]:

P-Q Load buses, in which the complex power consumption (given by P_i and Q_i) is known, but the voltage magnitude $|V_i|$ and phase angle θ must be determined. Often the reactive power is known from historical data or is based on an assumed power factor. Generators which can regulate their voltage must not be connected.

P-V Voltage-controlled buses, for which the real power P_i is known and voltage magnitude $|V_i|$ is kept constant, but the reactive power Q_i and phase angle θ_i must be determined. This is mostly true for generator buses but load buses may also have voltage control capability.

Slack As the voltage magnitudes and angles are initially unknown for some buses and resulting line losses need to be compensated, the power output of at least one generator bus must not be fixed. The voltage magnitude $|V_1| = 1.0\,\mathrm{p.u.}$[1] and angle $\theta_i = 0°$ of this bus serve as a reference so that angle specifications at all other nodes are possible. By this, an over-constrained system defining power injections for all buses is prevented and the system losses are assigned to the slack bus once they are known.

Additionally, to the bus classifications, the routing, and characteristics of the lines and transformers connecting the buses need to be given. The π-model represents lines as a simple network of passive components that can be easily analyzed using circuit theory. It assumes, their parameters (resistance, inductance, capacitance) are uniformly distributed (constant) along the length of the line. This model is commonly used to simplify the analysis of transmission lines. With this, the bus admittance matrix (Equation (2.1)) can be derived, which represents the nodal admittance relationships between all n buses in an electric power system and is used to calculate the power flow.

$$Y_{bus} = \begin{bmatrix} Y_{11} & Y_{12} & \cdots & Y_{1n} \\ Y_{21} & Y_{22} & \cdots & Y_{2n} \\ \vdots & \vdots & \ddots & \vdots \\ Y_{n1} & Y_{n2} & \cdots & Y_{nn} \end{bmatrix} \tag{2.1}$$

where Y_{ik} represents the negative sum of all admittances connecting bus i with bus k. The diagonal elements Y_{ii} represent the total self-admittance at each bus, which includes the sum of the capacitance and the load admittance. The off-diagonal elements Y_{ik} with i $\neq$ k represent

[1] in a per unit system

the mutual-admittance between pairs of buses, which are connected by lines or transformers. If buses are not connected, the value of their admittance is 0. A detailed derivation can be found in [28, Section 4.2.4], [26, Equation 6.4.2], [24, Section 19.2].

There exist multiple power flow representations and it is still an active research topic. The I-V power flow equations are derived from two fundamental properties of AC power systems. Equation (2.2), the linear association between voltage phasors and current injection phasors, and Equation (2.3), the definition of complex power. These characteristics are expressed mathematically for each bus $i \in \mathcal{N}$, resulting in the following equations based on the current law of Kirchhoff [29].

$$I_i = \sum_{k=1}^{\mathcal{N}} \mathbf{Y_{ik}} V_k \tag{2.2}$$

$$S_i = V_i I_i^* \tag{2.3}$$

substituting Equation (2.2), we obtain:

$$S_i = V_i \sum_{k=1}^{\mathcal{N}} \mathbf{Y_{ik}^*} V_k^* \tag{2.4}$$

From this, the PQV (Active-Power Injection, Reactive-Power Injection, Voltage magnitude) power flow equations can be formulated. It is primarily used for AC power flow analysis as it relates the real and the reactive power injections to the bus voltages and the complex admittance matrix of the system. Assuming that the bus admittance matrix Y_{bus} is known, the power flow equations are formulated as described in [28, Section 4.2.5], [24, Section 19.2.1], [29, Section 2.1.1] with an element of the bus admittance matrix Y_{ik} and the voltage of bus i defined by:

$$Y_{ik} = |Y_{ik}| \left(\cos \psi_{ij} + j \sin \psi_{ij}\right) \tag{2.5}$$

$$V_i = |V_i| \left(\cos \theta_i + j \sin \theta_i\right) \tag{2.6}$$

In Equation (2.4), we substitute Equation (2.5) and Equation (2.6) to obtain:

$$S_i = \sum_{k=1}^{\mathcal{N}} |\mathbf{Y_{ik}} V_i V_k| \cos\left(\theta_i - \theta_k - \psi_{ik}\right) + j \sin\left(\theta_i - \theta_k - \psi_{ik}\right) \tag{2.7}$$

This can be expressed in polar form as a combination of its real and reactive components:

$$S_i = P_i + jQ_i \tag{2.8}$$

$$P_i = |V_i| \sum_{k=1}^{\mathcal{N}} |\mathbf{Y_{ik}}| \, |V_k| \cos\left(\theta_i - \theta_k - \psi_{ik}\right) \tag{2.9}$$

$$Q_i = |V_i| \sum_{k=1}^{\mathcal{N}} |\mathbf{Y_{ik}}| \, |V_k| \sin\left(\theta_i - \theta_k - \psi_{ik}\right) \tag{2.10}$$

$$i = 1, 2, ...n; \quad i \neq \text{slack bus}$$

The equations that need to be solved to determine the variables of interest are non-linear making the problem not practical to a closed-form solution. However, an approximate solution is sufficient and iterative numerical methods like Gauss-Seidel can be employed to find an appropriate solution. In the context of this thesis, we will rely on the implementations of the toolkit `PyPSA` in order to conduct power flow analyses which uses the Newton-Raphson-Method [30]. It is a numerical technique used for solving a set of non-linear equations in an equal number of unknowns simultaneously. Using an iterative approximation of the solution by means of successive refinements based on the use of tangent lines:

$$x_{n+1} = x_n - \frac{f(x_n)}{f'(x_n)} \tag{2.11}$$

The method begins by selecting an initial guess for the solution, and then iteratively updating this guess until the desired level of accuracy is achieved. At each iteration the Jacobian matrix is calculated, which represents the first order derivatives of the defining state variables of the power flow equations. The Jacobian matrix is then used to update the solution at each bus in the power system. This process is repeated until a threshold of convergence is satisfied.

The convergence of the Newton-Raphson method depends on the choice of initial guess, the behavior of the function and its derivative (the diagonal dominance of the bus admittance matrix). The self-admittances at the busses are usually large, compared to the mutual-admittances. But junctions of long lines are detrimental to convergence as these tend to weaken the diagonal dominance [24]. However, this method can provide very accurate and fast solutions but is also very sensitive to the choice of initial guess and may fail to converge or converge slowly in certain cases. Most often, the fixed slack bus values are suitable as initial guess, since the final voltage solutions should not deviate significantly from the nominal values. When handling a series of related problems like multiple time steps, utilizing the previous solution has also proven good as initial guess [31].

2.2.2 Optimal Power Flow

In Section 2.2.1 we showed, how a feasible solution for a certain point of operation in the power grid can be determined while adhering to the necessary conditions. This is possible if all generation and load is given. Of further interest is the optimal dispatch of specific flexible components. This is known as the alternating current optimal power flow (AC-OPF) and used to determine the optimal use of these components due to a certain objective and subject to physical and technical constraints. Building on the derivations of the power flow equations, we will introduce an AC-OPF problem for the bus injection model (BIM) and explain the complexity of this problem. Using this as a basis, we will show how relaxations like branch flow model (BFM) can simplify the problem and where it is applicable.

The current on lines is a result of its voltage drop and the admittance between the two buses, described in Equation (2.12) by Ohms law.

$$I_{ik} = \mathbf{Y_{ik}}(V_i - V_k) \tag{2.12}$$

The complex power flow between buses i and k can be expressed as the product of the complex voltage at bus i, and the complex conjugate of the current flowing between the buses (Equation (2.3)). Therefore we can express the power transferred between buses i and k as:

$$S_{ij} = V_i I_{ik}^* = V_i \left(\mathbf{Y_{ik}^*}(V_i - V_k)\right)^* \tag{2.13}$$

Equation (2.14) expresses the law of conservation of power (energy). The total power injection into bus i has to equal the sum of power flows into and from bus i.

$$S_i = S_i^g - S_i^d \quad \forall i \in \mathcal{N} \tag{2.14}$$

With this, the basic form of the undirected BIM is formulated as:

$$S_i = \sum_{k \in \mathcal{N}} \mathbf{Y_{ik}^*}(|V_i|^2 - V_i V_j^*) \quad \forall i \in \mathcal{N} \tag{2.15}$$

We use the formulation of the BIM for the line flow (Equation (2.13)) and the partition of the complex power (Equation (2.8)) into its real (Equation (2.9)) and reactive (Equation (2.10)) component, upon which constraints and an objective function is formulated like in [29]. These are necessary to represent the operational limits in which the power flow problem should be optimized. An exemplary basic objective function $f(x)$ consists of the sum of the cost f_{Ci} of all flexible power generators P_{Gi} formulated in Equation (2.16) which we will minimize.

$$f(x) = \sum_{i \in \mathcal{G}} f_{Ci}(P_{Gi}) \longrightarrow min f(x) \tag{2.16}$$

The operational limits, already mentioned in the beginning of Section 2.2.1, are defined by maximum power values due to thermal limits of lines and transformers (Equation (2.17)) and limits to the capacity of the power generators (Equation (2.18) and Equation (2.19)). For a safe operation, voltage magnitude is usually bounded to a deviation of 10% or less (Equation (2.20)). It's important to bound the voltage angle within a range of $360°$ to guide the solver to a unique solution (Equation (2.21)). Also, the slack bus angle is fixed to zero (Equation (2.22)).

$$-\boldsymbol{S_{ik}^{\max}} \leq S_{ik} \leq \boldsymbol{S_{ik}^{\max}} \qquad \forall (i,k) \in \mathcal{E} \tag{2.17}$$

$$\boldsymbol{P_{g,i}^{\min}} \leq P_{g,i} \leq \boldsymbol{P_{g,i}^{\max}} \qquad \forall i \in \mathcal{N} \tag{2.18}$$

$$-\boldsymbol{Q_{g,i}^{\max}} \leq Q_{g,i} \leq \boldsymbol{Q_{g,i}^{\max}} \qquad \forall i \in \mathcal{N} \tag{2.19}$$

$$\left|\boldsymbol{V_i^{\min}}\right|^2 \leq |V_i|^2 \leq \left|\boldsymbol{V_i^{\max}}\right|^2 \qquad \forall i \in \mathcal{N} \tag{2.20}$$

$$-\boldsymbol{\theta_{ik}^{\max}} \leq \theta_i - \theta_k \leq \boldsymbol{\theta_{ik}^{\max}} \qquad \forall (i,k) \in \mathcal{E} \tag{2.21}$$

$$\angle V_1 = 0 \tag{2.22}$$

$$|V_1| = 1 p.u. \tag{2.23}$$

Representation of the power flow equations (2.24)

The formulation in Equation (2.15) leads to a non-linear feasible space for an optimal power flow (OPF) problem. Additionally, the lower and upper bounds of voltages in Equation (2.20) contribute to a non-convex solution space [32], making the AC-OPF problem an NP-hard problem, as demonstrated in [33] even for tree networks [34]. This means, in a non-convex solution space, there is no guarantee to achieve a global optimum without testing every point in the solution space, which makes convergence to a global optimum impractical for real-world network sizes. However, there are different approaches to mitigate computational complexity, such as relaxing some constraints to create a convex solution space, in which a polynomial time algorithm can find the global optimum or verify infeasibility. In this case, only the power flow equations (Equation (2.24)) have a non-linear character. Relaxations or approximations can transform them into a better solvable formulation with convex solution space. A detailed overview can be found in [29].

The BIM is the standard model for analyzing and optimizing power flow. It uses nodal variables, such as voltage, current, and power injections, while not directly representing the power flow on individual branches. Conversely, the BFM focuses on current and power flows on branches instead of nodal variables. Different convex relaxations have been studied using the branch flow models proposed in [35], [36]. As both models are descriptions of the Kirchhoff's laws,

their equivalence could be proven in [37]. The BFM equations are given:

$$p_j = P_{ij} - r_{ij} l_{ij} - \sum_{k:(j,k)\in\mathcal{E}} P_{jk} \qquad j = 1, ..., n \tag{2.25}$$

$$q_j = Q_{ij} - x_{ij} l_{ij} - \sum_{k:(j,k)\in\mathcal{E}} Q_{jk} \qquad j = 1, ..., n \tag{2.26}$$

$$v_j = v_i - 2(r_{ij} P_{ij} + x_{ij} Q_{ij}) + (r_{ij}^2 + x_{ij}^2) l_{ij} \qquad (i,j) \in \mathcal{E} \tag{2.27}$$

$$l_{ij} = \frac{P_{ij}^2 + Q_{ij}^2}{v_i} \qquad (i,j) \in \mathcal{E} \tag{2.28}$$

with r_{ij} and x_{ij} as resistance and reactance of the line ij respectively, p_j and q_j representing real and reactive total loads at node i. Due to the relaxation, new variables are introduced, namely $l_{ij} := |I_{ij}|^2$ being the squared current over line (i, j) and $v_i := |V_i|^2$ being the squared voltage magnitude of the complex bus voltage V_i, to emphasize linearity [38]. By this relaxed formulation, no phase angles of voltages and currents are included and therefore lost but they can be uniquely determined for radial networks [39], [40]. A simplified formulation called *DistFlow* was introduced in [41, Section 4.1] which we use in this work. This approximation can be used to determine the power flow in a radial distribution system. The quadratic term representing the losses in Equation (2.27) is dropped as they are much smaller than the active and reactive branch power terms, making it a linearized equation. The power losses can be approximated afterward. Other formulations are possible and depend among others on the power flow model, topology of the grid and detail of the model. In addition to the general grid constraints, further constraints can be introduced to define components more precisely and/or to investigate a certain behavior more closely. In this work, we focus on flexible loads such as HPs and BEVs, whose dispatch we optimize and therefore limit by constraining the solution space over their energy and power limits. Our implementation of the equations and constraints are described more detailed in Section 4.3.

2.2.3 Curtailment

To manage congestion, power system operators may curtail and reduce the output of certain generators or (in severe situations) request load shedding to reduce the demand for power in the affected areas. This helps to maintain the stability and reliability of the power system and prevent the risk of blackouts. As explained in Section 2.2, the power system must operate between certain limits. To do this, the conditions of Section 2.2.1 must be satisfied. In model-land, optimizing the component dispatch to stay within the set constraints may sometimes not be feasible. As we can see in Equation (2.17), maximum line or transformer capacities can be reached, forcing the power flow problem to fail, since we do not allow reinforcement for complexity reasons. As in the daily operation of DSOs, curtailment can be used in the

AC-OPF formulation to manage congestion. Curtailment can be implemented at high cost in the objective as a fallback option. Thus, the model could use it in case it would otherwise not be feasible. Feed-in is then curtailed until the maximum line or transformer capacity is reached, if not otherwise exceeded. Our implementation and the parameters for this approach are described in more detail in Section 4.3.

2.2.4 Reinforcement

As mentioned in Section 2.1.4, network reinforcement is a way to overcome network congestion and is necessary when components are operating at their limits. Reinforcement can be addressed in optimization through various approaches [42], although it is mainly used in TG expansion planning. Security Constrained Optimization Problems (SCOP) are used to find optimal expansion decisions [43]. However, this is not part of this work. We use the reinforcement heuristic of `eDisGo`[7], which is applied using fixed time series. `EDisGo` uses the power flow algorithm of `PyPSA`[30] with a single slack to determine the current state of the network. Line loads and voltage violations are then eliminated by network reinforcement. The applied allowed voltage deviations are listed in Table 2.2

Table 2.2: Allowed voltage deviation in `eDisGo` [7] for the MV-LV combined, MV only or LV only reinforcement. MV-LV station is only considered in LV only. The values are p.u.

	v_{rise}	v_{drop}
MV-LV	0.1	0.1
MV only	0.05	0.1
LV only	0.035	0.065
MV-LV station	0.015	0.02

For this purpose, standard reinforcement measures from the distribution network study [44] are applied to power lines and transformers. These are shown in Figure 2.4. The simplified procedure of the heuristic is as follows:

First, overloading issues are solved as they are less complex. To address these in power lines, a parallel line of the same type as the existing line is built. If not sufficient, additional parallel lines are installed stepwise until the overloading issue is mitigated. The same method is applied in solving overloading issues with transformers. Addressing voltage deviation issues is more complicated and needs to happen iteratively. The algorithm installs parallel standard transformers and conducts a power flow analysis after each measure until the issues are resolved. If there are multiple voltage deviation issues, the algorithm prioritizes the path with the highest voltage deviation and installs a parallel line to connect the transformer station and a node at 2/3 of the way along the path. Only one voltage deviation issue per feeder is considered at a time, and the process is repeated until all issues are resolved.

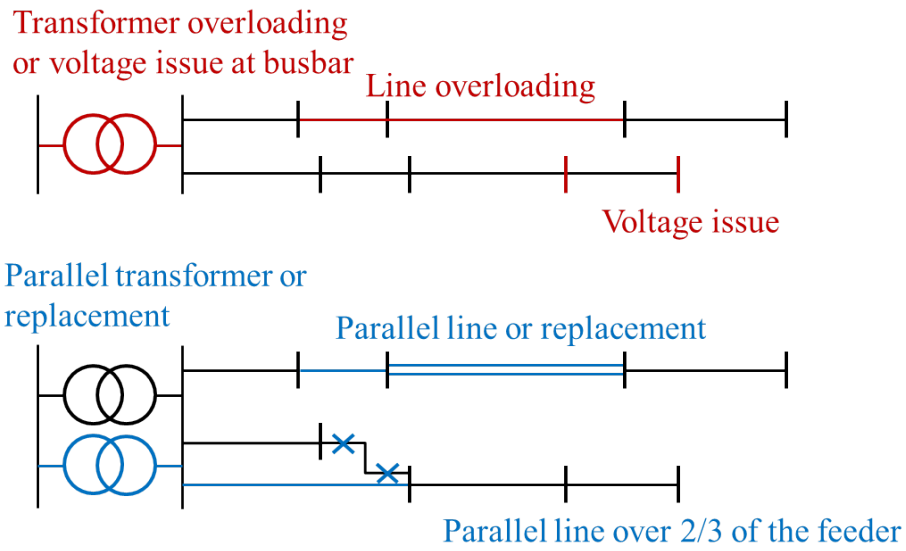

Figure 2.4: Grid reinforcement measures implemented in `eDisGo` to solve overloading and voltage issues [45]. The problem is defined in red and the solution in blue.

The costs of network expansion are determined on the basis of the measures taken to expand the network, with the relevant costs shown in Table 2.3. Transformer costs are differentiated only by voltage level, while cable costs are determined by both voltage level and the population density of the respective grid district, taking into account the higher costs associated with earthwork in more densely populated areas. The superscripts ^{a} and ^{b} mark the costs including earthwork in areas with a population density of $\leq 500 \frac{\text{people}}{km^2}$ or $> 500 \frac{\text{people}}{km^2}$ respectively.

Table 2.3: Costs for standard equipment [46] used for MV and LV networks in `eDisGo`

Equipment	**Overnight Investment Costs in kEUR**	**Unit**
MV cable, NA2XS2Y 3 × 1 × 185 RM/25	$20/80^a/140^b$	km
LV cable, NAYY 4 × 1 × 150	$9/60^a/100^b$	km
HV/MV Transformer, 40 MVA	1000	-
MV/LV Transformer, 630 kVA	10	-

For more detailed information on the basic reinforcement algorithm, we refer to the documentation of `eDisGo` [7] as this was not part of this work.

2.2.5 Flexibility Potential

Flexibility potential is a quantitative approach to measuring the degree of flexibility available in a system. It is expressed as a range of values that can be determined through various methods, such as modeling and simulation or empirical analysis. In the context of energy systems, flexibility potential can be quantified by analyzing the ability of different sources

of flexibility, such as energy storage or DR, to adjust energy consumption and production in response to changing conditions [47]. The available flexibility potential can be expressed in terms of the amount of energy that can be dispatched or stored over a given period of time.

D'hulst *et al.* defines the flexibility potential of aggregate appliances as a range between two bounds, as shown in Figure 2.5, which define a possible operating space. The bounds are represented by two lines, E_{max} and E_{min}, which represent the energy level of devices such as BEVs at a charging park (CP) when charging as early as possible and charging as late as possible, respectively. E_{max} and E_{min} define the flexibility bounds of the energy consumption of an aggregated group of flexible devices.

The figure shows two cases of the entire charging process compared to a reference process (green). In (a) there is an increase in power compared to the reference process and in (b) there is a decrease in power compared to the reference process. However, the reference processes are different in the scenarios. In the first scenario (a), the reference process (green) is when the energy consumption of the aggregated BEVs is shifted as much as possible, but would still meet their total demand at the end of time. The changed process (blue) is when the aggregated BEVs are suddenly charged with full power and reach their final energy demand much earlier. In the second scenario (b), the reference process (green) is when all BEVs are charged at full power, no consumption is shifted and each consumption is as early as possible. The changed process (blue) is when the power is suddenly reduced so that after ΔT the grouped devices reach the point where the power has been shifted as much as possible.

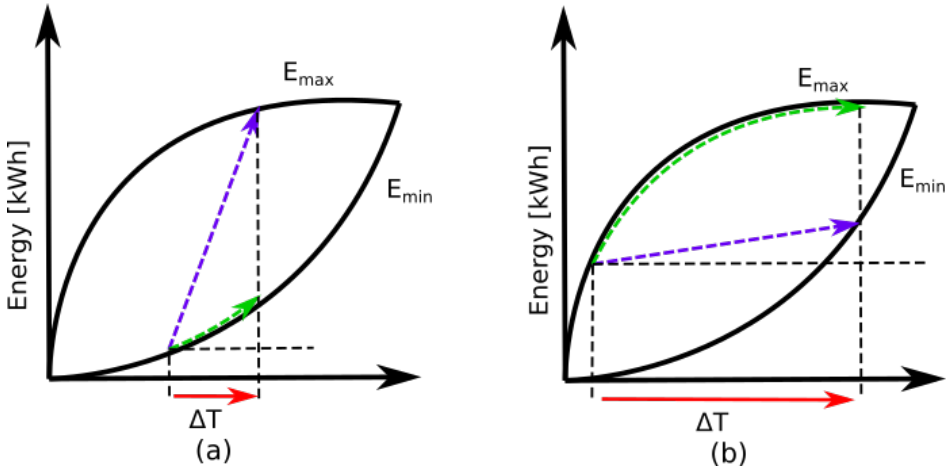

Figure 2.5: Illustration of the flexibility potential by energy level flexibility bands, with the green arrow, showing the reference process, and the blue arrow the adapted process. Two scenarios are shown: (a) increase of power consumption and (b) decrease power of consumption. [adapted from [47]]

These flexibility bands define the operating range of flexible devices. They can be used to constrain a variable in an optimization. We will call these flexibility bands flex-bands from

now on. The energy level flex-bands describe the perspective of all flexible devices. Since we are focusing on the whole network, the network perspective needs to be added. Therefore, the energy level flex-band is complemented by another flex-band describing the possible power consumption at each time step. This band describes the minimum and maximum power that all aggregated flexible units can consume without violating the grid constraints, regardless of their state of energy (SOE). By combining both flex-bands, the flexibility potential of the DG can be determined, taking into account the devices and the grid constraints.

2.3 Comparative Analysis

Several studies have examined the impact of vRES and flexible appliances on DGs. Gupta *et al.* modeled the impact of deploying PV, HPs, and BEVs on a Swiss LV DG and found that PV leads to more voltage violation issues compared to HP and BEV respectively which, on the other hand, cause slightly more line overloading. BESS however, have the potential to reduce expansion costs by up to 15% [48]. This finding is consistent with the results of Resch *et al.*, who also concluded that integrating PV and BESSs can reduce future grid expansion costs [49]. Furthermore, Scheller *et al.* found that DR and sector coupling options can further reduce storage capacity and decrease necessary investments [50]. In contrast, Rinaldi *et al.* analyzed the interplay of PV, HPs, and BESSs in Switzerland and found that more electrical storage is needed to decarbonize the heat sector. They also found that shifting HP operation into midday can improve PV deployment [51]. This suggests that there is a need for a coordinated approach to integrate different distributed energy resourcess (DERs) and storage systems for an optimal and efficient decarbonization strategy. Addressing this, Sinha *et al.* proposed a control system to manage HPs with TES and BEV charging systems in LV DGs to manage grid congestions [52]. This demonstrates that, with control system, DR can support managing grid operations with increased DER penetration. Moreover, Heider *et al.* analyzed multiple medium voltage grid district (MVGD) and found that the optimized operation of DERs can reduce grid reinforcement costs, but the extent differs depending on the combination of DER [53]. However, Veldman and Verzijlbergh caution that market-oriented charging of BEVs can increase network costs, particularly in high wind penetration scenarios [54]. Therefore, it is important to consider specific combinations of DERs and the effects of different market designs on DG operations. For this, quantifying the flexibility potential for DER is necessary. Saavedra *et al.* proposed a framework and mathematical formulation for demand aggregator-end-user interactions based on flexibility bands [55]. D'hulst *et al.* quantified the DR flexibility of residential smart appliances and derived flexibility bands based on real measurements in Belgium, but only on a small scale [47]. Stinner *et al.* developed a method to quantify the flexibility of building energy systems with TESs. Additionally, the option to aggregate the different flexibility measures on a city district level is addressed to gain more impact [56]. These results suggest that the flexibility of the DR can play a significant role and that aggregation increases the effect.

In summary, the studies show that to decarbonize all sectors and integrate renewables into the power system, DR is an additional method besides grid reinforcement. However, grid reinforcement is necessary in the course of sector coupling, but can likely be reduced by DR. To determine the flexibility potential of devices and the impact of DRs on the grid infrastructure, several approaches exist. Though, there seems to be a lack of research on the interplay between additional grid reinforcement and flexibility. Grid reinforcement is most often seen as a ”have to” rather than an enabler of DR flexibility. Moreover, flexibility is primarily analyzed for devices in the distribution system rather than aggregated and at the interface with the transmission system. Therefore, we aim to address this research gap by investigating the impact of grid reinforcement on flexibility potential. To do so, we focus on aggregated distribution system flexibility determining flexibility bands at the substation level.

3 Data

The investigation is based on the results of open data models like `ding0`, `feedinlib`, `demandlib`, `TracBEV`, `SimBEV` and `eGon-data` which have most of their datasets freely available on the Open-Energy-Platform. To begin, the individual datasets need to be integrated, as shown in Figure 3.1. The `ding0` grid topology, which describes the routing of lines and substations, is the foundation (Section 3.1) to which all power generation and demand components are connected (Section 3.2). The data for flexible demand components such as battery electric vehicles (BEVs) (Section 3.3) and heat pumps (HPs) with thermal energy storages (TESs) (Section 3.4) are described separately and in more detail.

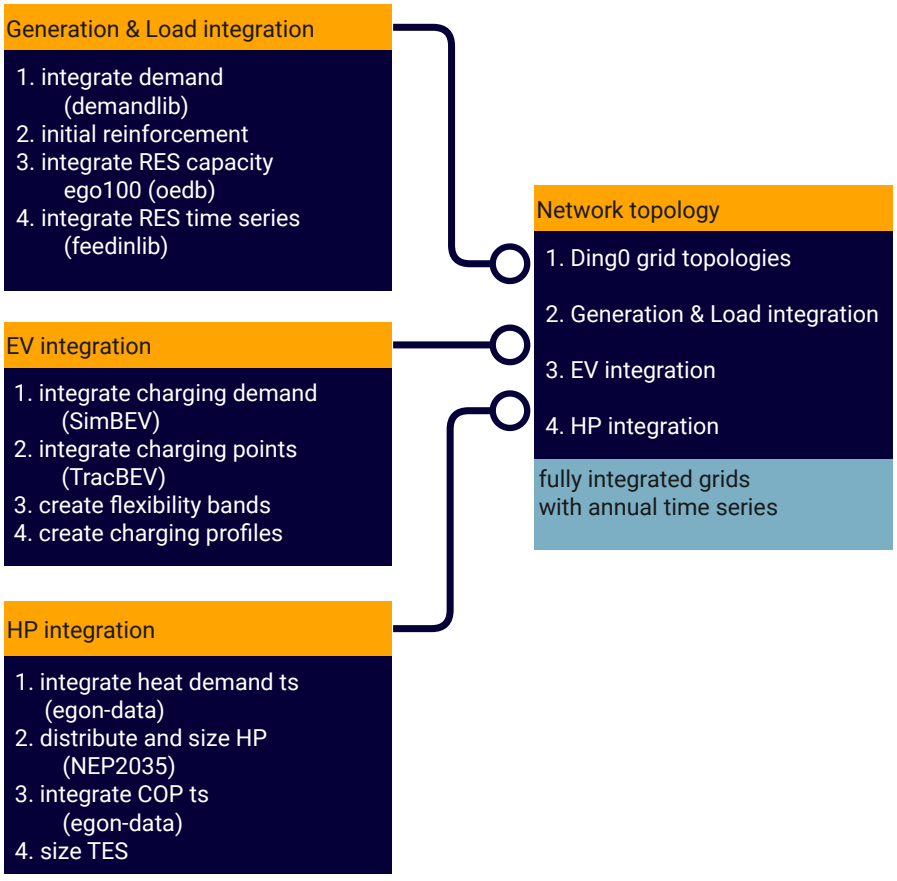

Figure 3.1: Process workflow for creating the networks and mapping the data

3.1 Grid Topology

We investigate synthetic medium voltage (MV)-low voltage (LV) grids generated with the distribution network generator `ding0`[57]. The tool synthesizes georeferenced MV grid topologies with underlying LV grids for entire rural and suburban Germany on freely available GIS-data as illustrated in Figure 3.2.

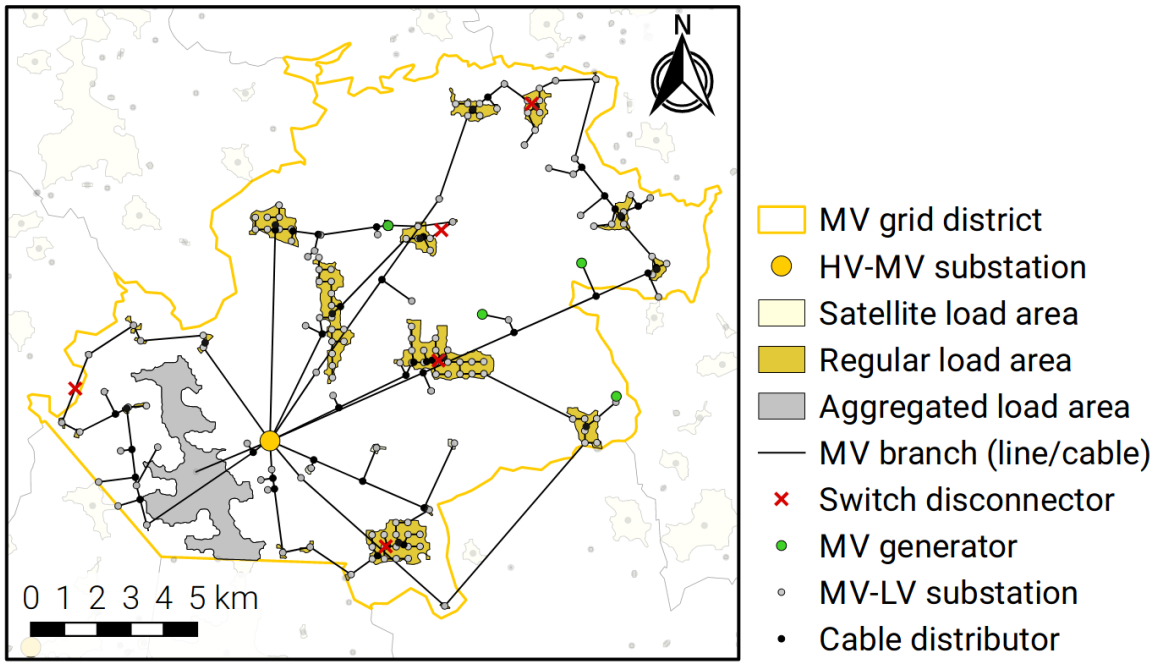

Figure 3.2: Example topology of a medium voltage grid district (MVGD) generated in `ding0` [6]

Based on data from Hülk *et al.*[58], the residential, agricultural, industrial, and retail sectors are mapped with a focus on peak demand to determine line capacity. Demography, land use and valid planning principles of MV grids are integrated, and the line routing is based on infrastructure data from OpenStreetMap (OSM). For this, an algorithm for a capacitated vehicle routing problem (CVRP) is used. MV grids are represented by open-ring topology to satisfy the $(N-1)$ failure criterion. An exemplary MV topology of a network is shown in Figure 3.2. For LV grids, sector typified grids with a radial network topology are used. Due to lack of freely available data, the grids do not claim to represent real grids but ones with sufficiently high similarity for research purposes [6]. To reduce the amount of 3608 MV-distribution grid (DG) with underlying LV grids [57], the results are clustered using the k-means-algorithm, identifying 15 representative grids [59]. From these, respectively two grids with characteristics defining a load, photovoltaic (PV) and wind dominated region are selected as shown in Figure 3.3[60]. The number of underlying LV grids, the covered surface area and the total line length for each MVGD is listed in Table 3.1. Since we are using `ding0`'s old grids in this work, there are still some existing artifacts that need to be reworked. `ding0` used to connect household loads and rooftop PV systems by one-meter end lines. These end

lines within the graph, which are smaller than one meter, are removed because they have no inherent use.

Table 3.1: Number of underlying LV grids, covered surface area and total line length per grid.

	1690	1811	1056	176	177	2534	unit
lv-grids	179	381	130	196	110	56	-
surface area	529	1665	445	308	145	62	km^2
line length	689	1515	474	881	556	341	km

3.2 Conventional Load & Generation

The renewable energy capacities used in the model are based on the eGo100 scenario of the scenario framework project *open_eGo* [61]. The scenario describes a future electrical energy system in Germany that is supplied by 100% renewable energy sources (RES).

Based on the status quo in 2015, the generation capacities, shown in Table 3.2 are regionalized and weighted according to the current distribution. Due to the complexity and lack of detailed information, generic solar and offshore wind power plants (PPs) are used. Onshore wind PP, on the other hand, are differentiated according to seven power classes that characterize typical onshore wind PPs in terms of installed capacity and location. The regionalization of the generation capacities and a detailed description of the methodology is included in the final report of the project [62, Section 3.1, 3.2].

Table 3.2: Total power generation capacity in Germany in 2035 according to the eGo100 scenario [62, p. 29]

Source	Total	Unit
Wind Onshore	98.4	GW
Wind Offshore	27.8	GW
Photovoltaic	97.8	GW
Biomass	27.8	GW
Hydropower	3.2	GW

For the household power demand, the *demandlib* [63] tool is used, which scales standard load profiles from the German Association of Energy and Water Industries (BDEW) and has an integrated API in *eDisGo*. The resulting electricity load profiles contain time series of hourly conventional electricity demand for the residential, commercial, agricultural, and industrial sectors. The time series data for the generation is taken from the Open-Energy-Platform (OEP)[64] for the year 2011. All PP of biomass and hydropower generation are assumed to be constant at full power as they are not optimized in the model. Figure 3.3 visualizes the installed capacities of variable renewable energy sources (vRES) and dispatchable renewable

energy sources (dRES) as well as the peak load of conventional loads, HPs and BEVs. Here you can see the different characteristics of the grids already mentioned in Section 3.1. MVGD 1690 and 1811 are clearly dominated by installed wind capacity, while 1056 and 176 have strong PV capacity. Networks 177 and 2534 have high peak load values. These characteristics have a fundamental influence on the behavior of the networks and are therefore useful to keep in mind when analyzing them.

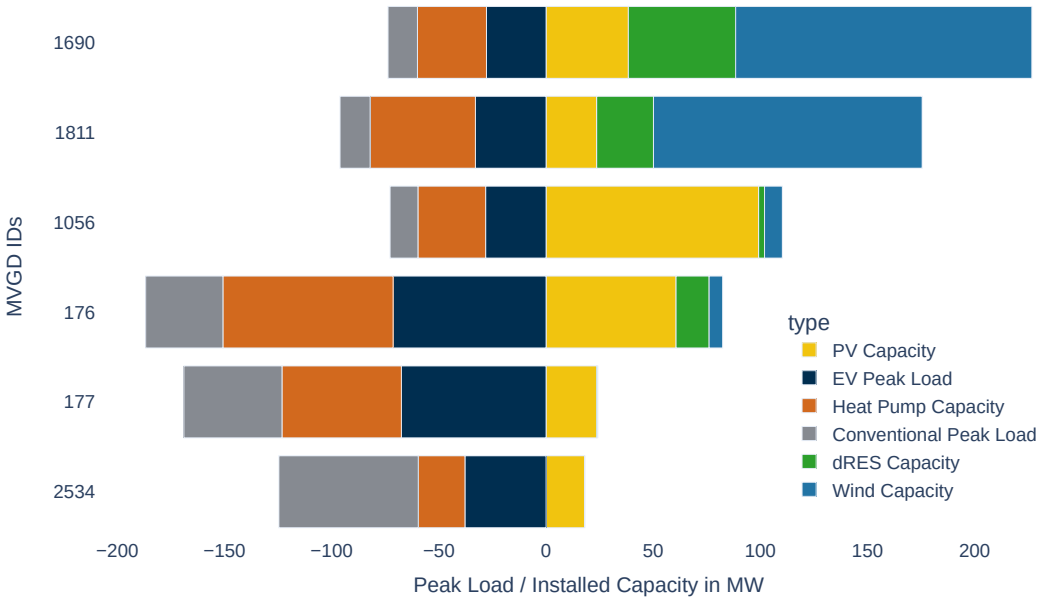

Figure 3.3: Installed generation capacities and peak loads for all selected MVGDs

3.3 Electric vehicles

The BEV scenario is based on the NEP C 2035 scenario of the German network development plan (NDP) 2019 [65]. The total number of BEV are used and disaggregated to the selected MVGDs based on current statistic on registered vehicles in Germany [66]. Trip profiles for individual BEV of various classes are created in `SimBEV` using a probabilistic approach based on the Mobilität in Deutschland (MiD) 2017 Survey [67]. A heuristic is applied to create charging processes for electric vehicles in 15-minute intervals, based on the trip profiles. BEVs may also be charged outside their assigned geographic areas, particularly during commuting and holiday travel, which is not directly represented in this study. We assume that these effects cancel out between regions. The results provide information on the start and end of trips, as well as the distance travelled, from which standing times and charging demand are derived. `TracBEV` is then used for the distribution of charging parks (CPs) within the geographic area. The charging structure is classified into public and private locations, whose charging processes are handled differently. The private infrastructure includes charging at home and at work, and

potential charging locations are identified based on the number of housing units in the area or the land use classification from OpenStreetMap. The public infrastructure is classified into normal and uncoordinated charging (in the following named *direct-charging*), with potential charging locations identified based on points of interest in the area or existing gas stations. The number of CPs for each location is determined based on the ratio of electric vehicles in the network area and the number of possible connection points, with a maximum number of CPs assigned to each connection point. The allocation of the charging processes to the charging infrastructure is carried out with a weighted random selection. For connections with a power up to 300 kVA, the integration is done in the LV-level to the closest transformer in the network, while higher power connections are done directly in the MV-level to the nearest network node or cable. A more detailed description about the methodology can be found in the master thesis of Helfenbein [68] as this was not part of this work.

The obtained time series of a whole year with 15 min resolution are resampled to hourly mean values. Energy level and power flexibility bands (introduced in section 2.2.5) for home and work charging points are generated, which define the flexibility potential. An example for eight aggregated charging points is illustrated in Figure 3.4 with energy band (red) and power band (blue). The charging power ranges between zero and the total charging power of all connected BEVs. The lower energy bound represents a charging pattern where the BEVs are left uncharged as long as possible to be charged at full capacity during the final time steps of their stationary period. Conversely, the upper energy bound corresponds to a pattern of *direct-charging* at full capacity until the required charging level is achieved.

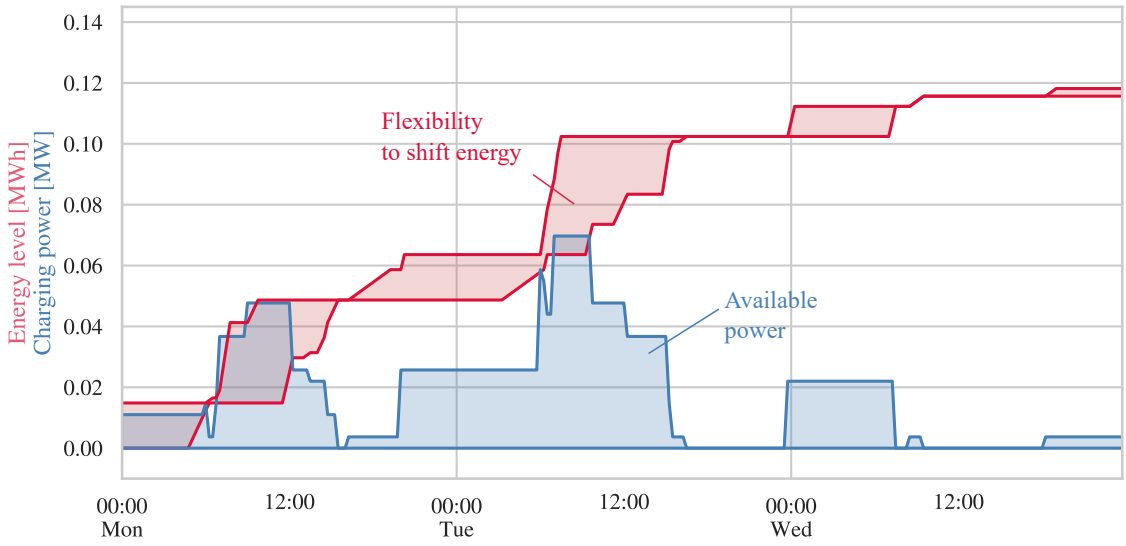

Figure 3.4: Flexibility band for BEVs. Lower and upper bounds of charging power and energy level at an exemplary charging location with multiple CPs [60].

Within this approach, charging events are considered to be independent. Shifting of charging events between multiple standing times is not possible. Additionally, time-series are created for all charging point types, using the *direct-charging* pattern, which describes an immediate full

power charging process of each BEV. These time-series are only used for inflexible charging points (public and high power charging (HPC)). In our reference scenario, however, all charging points are considered inflexible. Furthermore, the time-series are also used to calculate the residual load to determine the observation periods (described in Section 4.2.1). Table 3.3 provides an overview of the installed capacity of charging points in the several MVGDs. The installed capacities are very similar, but the number of installed charging points differ. The high capacities relate to the HPC parks.

Table 3.3: Installed charging park capacity in each network

	2534	176	177	1056	1690	1811	Unit
count	1747	3293	3094	1228	1230	1450	-
min	3.70	3.70	3.70	3.70	3.70	3.70	kW
50%	22.00	22.00	14.70	22.00	22.00	22.00	kW
max	500.00	350.00	500.00	500.00	500.00	500.00	kW

3.4 Heat Pumps & Thermal Storage

We assume that HPs are predominately installed in residential buildings. Within the eGon project, HPs are all of the type air source. To define the number of buildings with HPs, we assume a uniform distribution within Germany. The share of 38,13 % is derived from the projected number of HP (7 Mio) in the NEP C 2035-scenario of the NDP [65] and the number of residential buildings in 2021 [69]. Heat pumps are added to selected existing residential loads. The annual heat demand profiles are obtained from the data model of the *eGon* project [5], [70] and are based on bottom-up load profiles for space-heating and domestic hot water. These profiles have been regionalized and scaled [71]. Corresponding coefficient of performance (COP) time series for air-source heat pumps are also obtained from *eGon* data model [5], [70]. As the load areas differ in the *eGon* project, the regionalization cannot be transferred to this work, so profiles have to be randomly selected from a MVGD with a similar number of residential buildings.

Due to the wide range of profiles available, only profiles within an annual amount of 8-20 MWh are extracted. The eGon dataset also includes profiles for urban buildings. Therefore, we try to filter for profiles within a rural and suburban range. This range is determined by specific heat demand 80 $\frac{\mathrm{kWh}}{\mathrm{m}^2}$ (EnEV 2009) and 100-250 m^2 of living space [72].

Based on the annual profiles, the HPs installed thermal power P_h^{th} is determined:

$$P_h^{th} = \frac{24h}{24h - T_{day}^B} \cdot \max(\dot{Q}_t^D), \qquad T_{day}^B = 6h, \tag{3.1}$$

$$P_h^{nom} = \frac{P_h^{th}}{\mathrm{COP}(t_{\dot{Q}_{max}})}, \qquad \forall\ h \in \mathrm{HP}. \tag{3.2}$$

Most HPs are operated at a reduced heating tariff, which allows grid operators to impose 6 hours of blocking a day T_{day}^{B}. To cover these, and allow some flexibility in times of high heat demand, the heat pump is oversized. We introduce a flexibility factor to account for the blocking, which is multiplied by the maximum heat demand $\max(\dot{Q}_t^D)$. The electrical nominal power of the HP P_{hp}^{nom} is derived with the COP at the respective time step of maximum heat demand $t_{\dot{Q}_{max}}$. It is assumed that every HP is built with TES which is sized to cover the six consecutive hours with the highest total heat demand of each building. Again, six hours are chosen to cover the potential blocking time of the grid operators.

$$C_{hp}^{TES} = \max\Big(\Big[\sum_{t=i}^{i+6}(\dot{Q}_t^D)\Big]\Big) \text{ for } i \in \{0, 8760-6\} \qquad \forall i \in N,\ \ t \in T,\ \ h \in \mathrm{HP}. \tag{3.3}$$

The capacity of TES is rounded to the next higher $5\,\mathrm{kWh}_{th}$ and HPs to the next higher full kW_{el} to obtain regular sizes which are similar to market size capacities. The resulting distributions are illustrated in Figure 3.5. Finally, time series are generated for use in the reference scenario, where all HPs are assumed to be inflexible. Therefore, the operation strategy assumes that the heat demand is served directly by the HP without using the TES.

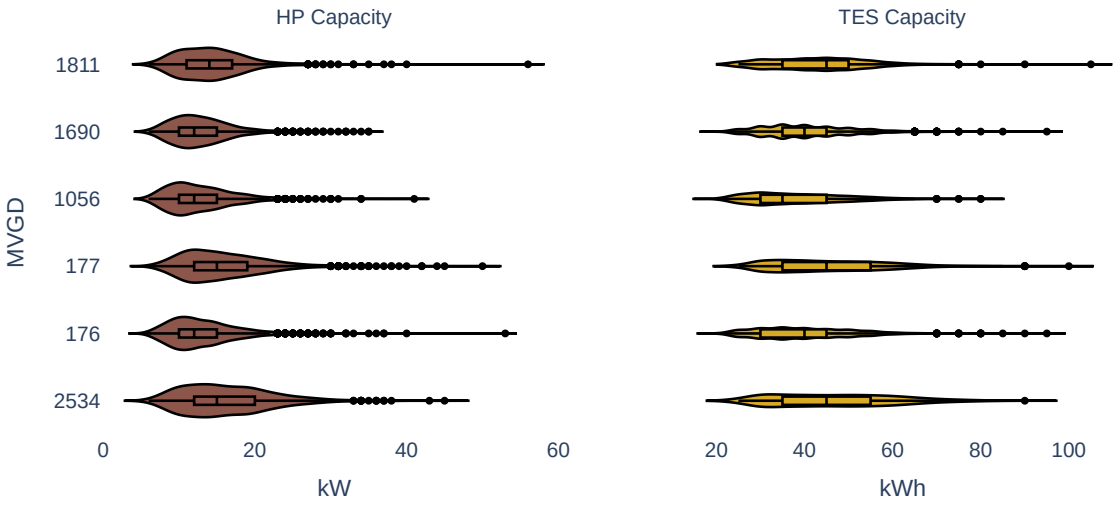

Figure 3.5: Distribution of installed HP and TES capacities per grid.

4 Methodology

In this chapter, the methodology used to identify the flexibility potential of distribution networks is described. The general procedure and goal are first introduced (Section 4.1). Next, the applied techniques of spatial and temporal decomposition are explained and reasoned (Section 4.2). The optimization model is then described in detail, including the objective for minimal line loading and the representation of the grid, generation, and load components (Section 4.3). The approach for load balancing potential and its further objective are introduced (Section 4.4). Finally, the different reinforcement scenarios on which this approach is applied, is described in Section 4.4.3.

4.1 Goal & Procedure

The workflow presented in Figure 4.1 outlines our methodology for determining the minimum required reinforcement and subsequent flexibility potential that the distribution networks can provide to the transmission system after additional reinforcement using flexible demand components such as heat pump (HP) and battery electric vehicle (BEV). Synthetic `ding0` networks consisting of conventional loads, renewable energy sources (RES) capacities from the *ego100* scenario, and BEV and HP data are used. The included annual hourly time series refer to the projected horizon of 2035. First, observation periods are identified using residual load as an indicator of network condition. For each network, two periods are identified to examine either the need for reinforcement or the potential for flexibility provision. To investigate the minimum reinforcement required, the dispatch of flexible components is optimized using a minimum line loading objective. Prior to all optimizations, the network feeders are separated to parallelize their computation. The determined dispatch time-series are then used to reinforce the individual networks. The results of the minimum line load reinforcement are compared with those of a reference scenario, which assumes immediate charging of all BEVs and direct use of HPs to satisfy heat demand. Building on the minimal reinforcement scenario, five additional scenarios are defined, representing a situation in which the load is supplied solely by the overlying network. The load of all flexible units is incrementally increased by 20 %. The reinforced networks are optimized using minimum and maximum objectives for both power and energy levels. The resulting time series are combined to characterize the flexibility of all aggregated HPs and BEVs using flex-bands.

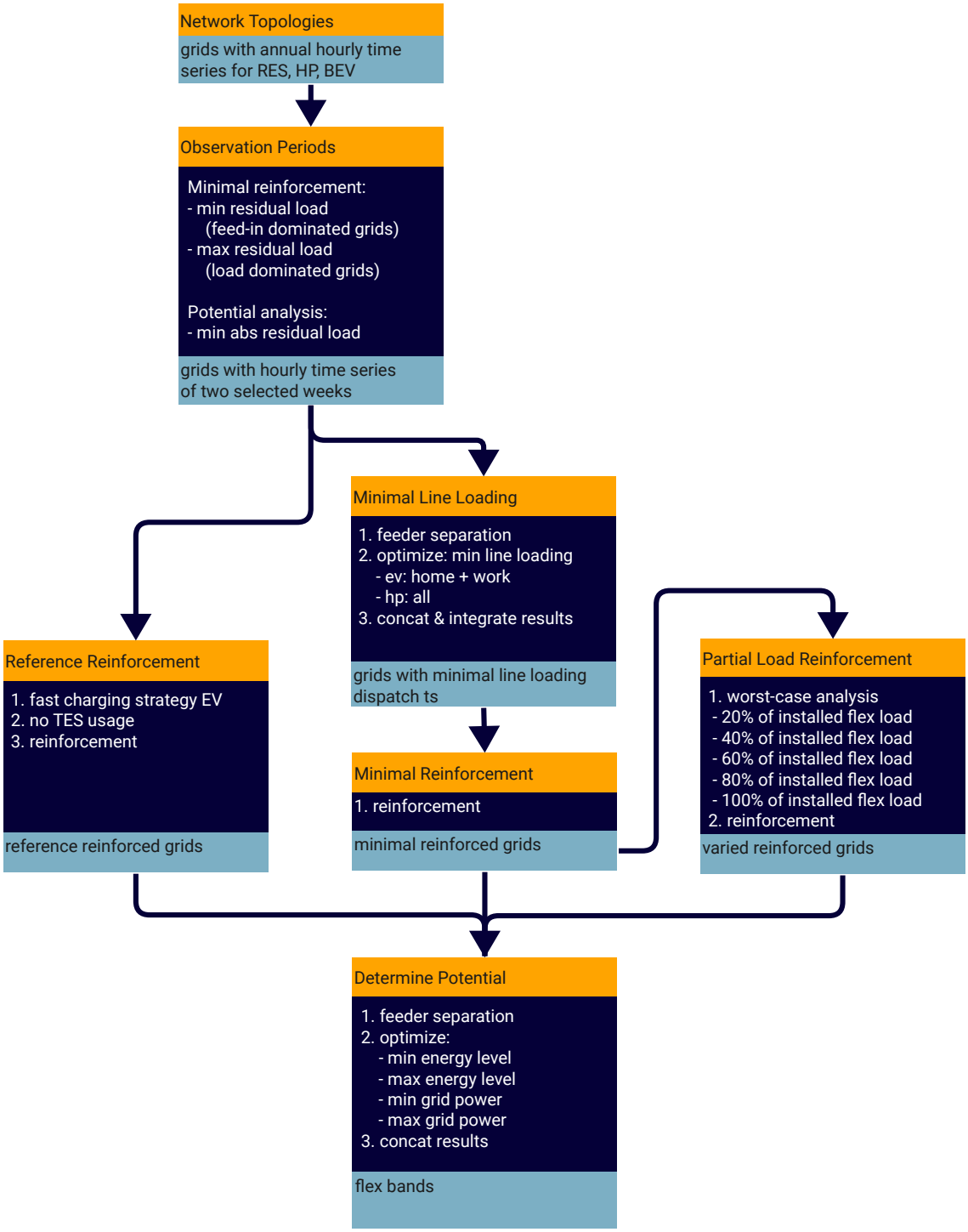

Figure 4.1: Process workflow diagram describing the several steps to determine the load balancing potential.

4.2 Spatio-temporal decomposition

In many cases, optimization problems are complex and difficult to solve directly. Decomposition can help by breaking the problem into smaller subproblems with less memory that are easier and faster to solve, and then combining the solutions. This even allows parallelization of the subproblems, use of multiple kernels, and increased time efficiency. Temporal decomposition is a process of breaking down time-series data into separate parts that capture different aspects that can be analyzed separately. This was achieved by choosing representative observation periods. Further, we used a spatial decomposition, which involves dividing a space into distinct parts. It is important to ensure that these divided parts are independent of each other in order not to alter the results. This was applied by dividing the medium voltage (MV) power grid into its separate feeders.

4.2.1 Observation periods

To determine the flexibility potential within the distribution system, we analyze the use of flexibility over a period of two independent weeks per grid. This approach was chosen to reduce computational amount and focus on the critical weeks which are most revealing. The observation periods were identified by examining different stages of residual load. The residual load is defined as the difference between the total demand p_t^D and the total generation p_t^G:

$$p_t^R = \sum_{n \in \mathbf{N}} p_{n,t}^D - \sum_{n \in \mathbf{N}} p_{n,t}^G \qquad \forall t \in T. \tag{4.1}$$

Therefore, a positive residual load p_t^R represents a load case while a negative residual load represents a feed-in case. To approximate which weeks are suitable, we took the sum of the residual load of a week p_{sum}^R as a reference. This was done using a rolling window approach with full-day increments, always starting at 0 AM as defined in the following equation:

$$p_{i,\text{sum}}^R = \sum_{t=24\cdot i}^{24\cdot(i+7)} \begin{cases} p_t^R & \text{load/feed-in case} \\ |p_t^R| & \text{flexibility case} \end{cases} \qquad \forall\, i \in \{0, 365-7\} \in \mathbf{N},\ \ \forall t \in T. \tag{4.2}$$

We aim to identify a specific type of week for the minimal reinforcement. In the case of a load-dominated network, with high positive p_{sum}^R and in the case of a feed-in-dominated network, with high negative p_{sum}^R. In both cases, we assume the grid infrastructure to experience maximum stress as power needs to be transmitted from or to the higher-level grid. Furthermore, we want to analyze the maximum flexibility that can be transferred to the transmission system. We assume that a week with minimal absolute residual load provides the greatest degree of freedom. When generation and demand are almost balanced within the MV grid, no additional power demand from or to the substation needs to be supplied. This is when

we expect the distribution grid to provide maximum short-term flexibility to the transmission grid in both positive and negative way. Therefore, we differentiate between the following three cases to identify two observation periods per grid depending on their characteristic as load or feed-in dominated.

4.2.2 Feeder Separation

Feeder separation is a process of spatial decomposition that allows the separate examination of MV electrical feeders. This process is only applied in order to parallelize tasks in the optimization and reduce computation time significantly. The grid is split into main feeders that run downwards from the HV/MV substation, including their low voltage (LV) subnetworks and all components. Radial lines are split at their switches into two separate feeders. During separation, graphs with only one sub node are neglected, as there are no flexible loads connected at MV-level, and therefore they do not need to be optimized. The feeders only common point is the substation where the loads are aggregated, thus they do not affect one another. After the optimization tasks, the results are merged and the optimized dispatch is integrated into a full grid for further steps.

4.3 Dispatch Optimization

We optimize the dispatch of BEVs & HPs to determine time series that describe the use of grid-supportive flexible demand units. For this, a preexisting model for a single linear programming problem was used [53], [60] and adapted for our use. The resulting time series are later used to define a minimal reinforcement required for the given penetration of BEVs and HPs. First, we introduce the model objective, before describing the grid model, which represents the network topology, all inflexible generation and demand components. The flexible components themselves are described separately due to their individual implementations. The model is written in *Python* and integrated into `eDisGo`[7] using `Pyomo`[73] as the optimization modeling language supporting several solvers. An academic license of Gurobi[74] was used in this work.

4.3.1 Objective

To determine the flexible demand unit dispatch, we minimize the quadratic objective described in Equation (4.9). The objective is defined by the squared component loading $l_{b,t}^2$, which is the ratio of the active power flow on a branch $p_{b,t}$ and the maximum active power $P_{b,t}$. It also minimizes the required curtailment $p_{n,t}^{curt}$ at each node to keep the power flow within the allowed grid bounds (eqs. (4.6) to (4.12)).

$$\min_{p,q,\dot{q},e,soe,v} \delta_{curt} \sum_{t\in T}\sum_{n\in N} p_{n,t}^{curt} + \delta_{load} \sum_{t\in T}\sum_{b\in B} l_{b,t}^2 \qquad \text{with} \qquad l_b = \frac{p_{b,t}}{P_{b,t}}, \tag{4.3}$$

$$\delta_{curt} = 10^{-2} \qquad >> \qquad \delta_{load} = 10^{-5}. \tag{4.4}$$

We have chosen $\delta_{curt} = 10^{-2}$ and $\delta_{load} = 10^{-5}$ as the weighting factors, so that curtailment is used as a secondary consideration. The curtailment at each node $p_{n,t}^{curt}$ is defined by the weighted sum of the active power curtailments $p_{n,t}^{curt,l}$, $p_{n,t}^{curt,EV}$, $p_{n,t}^{curt,HP}$, and $p_{n,t}^{curt,f}$ of the loads, BEVs, HPs, and feed-in, respectively:

$$p_{n,t}^{curt} = \delta_{curt,l}\, p_{n,t}^{curt,l} + \delta_{curt,EV}\, p_{n,t}^{curt,EV} + \delta_{curt,HP}\, p_{n,t}^{curt,HP} + \delta_{curt,f}\, p_{n,t}^{curt,f}. \tag{4.5}$$

with fixed weighting factors $\delta_{curt,l} = \delta_{curt,HP} = 1$ and $\delta_{curt,EV} = \delta_{curt,f} = 0.5$ to prefer curtailment of feed-in and BEVs over HPs and conventional load. To simplify the problem, we assume that the flexible loads do not draw any reactive power and that the reactive power curtailment of the load $q_{n,t}^{curt,l}$ (shedding) and the feed-in $p_{n,t}^{curt,f}$ (spilling) follow proportionally. Since we do not focus on reactive power provision, this assumption is appropriate. Minimizing the component loading $l_{b,t}$ is an indirect way to limit grid reinforcement, and is therefore used in this scenario. The optimization is performed for each feeder individually, the results are subsequently combined and then applied to the network as a whole.

4.3.2 Grid model

We use the simplified *Dist-Flow*[41] model introduced in Section 2.2.2 to represent the network. This approximation is only applicable to radial networks and as MV grids are operated as an open ring and the LV grids are radial, this approach is permissible. To be able to use a linearized model, we neglect the line losses which represent the second order term as proposed by Baran and Wu[41]. Line loses can be approximated ex post [41], but this was not yet implemented in the model and is also not the aim of this work. In addition, we do not use voltage controlled generators, but instead implement generators with fixed time series for active and reactive power due to their low generation capacities. This approach is common in distribution grids (DGs) and also used in `eDisGo`[45, p.14]. Thus, the following set of power flow equations for active $p_{b,t}$ and reactive power $q_{b,t}$ on all branches B and time steps T is used similar to [60] but extended for HPs:

$$p_{b,t} = \sum_{n \in down(b)} \left(P_{n,t}^{fix} + p_{c(n),t}^{EV} + p_{c(n),t}^{HP} - p_{n,t}^{curt,l/BEV/HP} + p_{n,t}^{curt,f} \right), \tag{4.6}$$

$$q_{b,t} = \sum_{n \in down(b)} \left(Q_{n,t}^{fix} - q_{n,t}^{curt,l} + q_{n,t}^{curt,f} \right) \qquad \forall t \in T, \;\; b \in B. \tag{4.7}$$

For this purpose, the power of all nodes $n \in down(b)$ downstream in the radial network is drawn from the branch b. The active and reactive power of all inflexible units is summed at node n and represented by $P_{n,t}^{fix}$ and $Q_{n,t}^{fix}$. $p_{c(n),t}^{BEV}$ and $p_{r(n),t}^{HP}$ describe the flexible charging power of the charging park c and the residential building r connected to the node n, respectively. To allow some flexibility in the grid, we allow curtailment which is described by $p_{n,t}^{curt,f}$ for feed-in and $p_{n,t}^{curt,l/BEV/HP}$ for load, BEV and HP. The reactive power curtailment for load $q_{n,t}^{curt,l}$ and $q_{n,t}^{curt,f}$ are assumed to follow proportionally, as power factors for loads and generators stay constant. Also, we assume a power factor of $cos(\phi) = 1$ for the flexible units, so they don't appear in the reactive power equation. As reactive power provision is not the focus of this study, it is not optimized. For this reason, only the resulting total active power at node b needs to be constrained (Equation (4.8)) by the maximum active power $P_{b,t}$ in both directions.

$$-P_{b,t} \leq p_{b,t} \leq P_{b,t}, \tag{4.8}$$

$$P_{b,t} = \sqrt{\left(S_b^{nom}\right)^2 - \left(Q_{b,t}^{fix}\right)^2} \qquad \forall t \in T, \;\; b \in B. \tag{4.9}$$

$P_{b,t}$ is approximated by the thermal limit S_b^{nom} of the branch b and the total reactive power flow $Q_{b,t}^{fix}$ of all inflexible units downstream. The $(\mathcal{N}-1)$ failure criterion, which should cover a component failure, is not taken into account. Besides the line flows, also the relationship between the nodes n is described. The following equations are used to define the node voltages:

$$v_{slack,t} = V_{nom}^2 \qquad \forall t \in T, \tag{4.10}$$

$$v_{m,t} = v_{n,t} + 2 \cdot (p_{b,t} \cdot R_b + q_{b,t} \cdot X_b) \qquad \forall t \in T, \;\; b \in B, \tag{4.11}$$

$$V_{min,l}^2 \leq v_{n,l} \leq V_{max,l}^2 \qquad \forall n \in N, \;\; l \in \{lv, mv\}. \tag{4.12}$$

The slack $v_{slack,t}$ at the MVHV-Station is set to the squared nominal voltage of the grid. The voltage drop between two neighboring nodes m respectively n is defined in Equation (4.11) with resistance R_b and reactance X_b of branch b. As we compute both voltage levels together, we need to convert the LV impedance to the MV reference system beforehand.

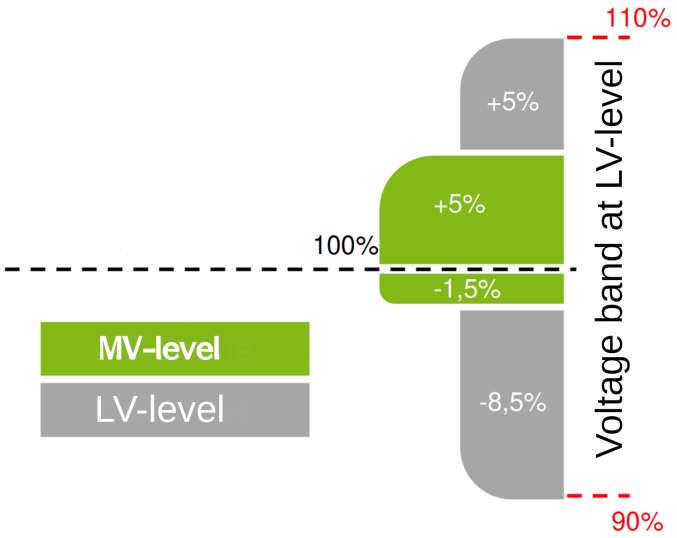

Figure 4.2: Voltage band division for MV and LV level [altered after [44]].

In addition, *EN 20160* [75] describes the minimum requirements for voltage quality at the consumer level, and thus defines the permissible voltage variation at the LV end user for ± 10% of the nominal voltage V_{nom}. According to Rehtanz *et al.* [44, p. 39], we divide the voltage band for the individual levels and define upper and lower limits. At the MV level, the upper limit is defined with a tolerance of 5% based on the reverse flow case. At this level, more generation capacity is connected, thus a larger share is claimed. Conversely, more load is connected at the LV level, so the lower limit of 1.5% at the MV level is sufficient. This gives us a more detailed formulation of Equation (4.12) for each voltage level:

$$(0.9\ V_{nom})^2 \leq v_{n,lv} \leq (1.1\ V_{nom})^2, \tag{4.13}$$

$$(0.985\ V_{nom})^2 \leq v_{n,mv} \leq (1.05\ V_{nom})^2. \tag{4.14}$$

4.3.3 Electric Vehicles

As described in Section 3.3, the flexibility of electric vehicles is defined by their standing time and demand at specific locations. We consider public and high power charging (HPC) stations as *direct* charging, as short standing periods are assumed. This means vehicles are charged with full power as soon as they are connected to the charging station. Thus, their demand can not be made flexible and therefore active power time-series are provided. Whereas home and work charging is considered as flexible charging, as long-standing time periods are assumed. Flexibility bands describe the operational space within the charging at each location are optimized (Figure 3.4 in Section 3.3). One band defines the energy level, another the power consumption. By this approach, charging processes are considered aggregated at each location. The aggregated bands are obtained by adding the individual upper and lower bands. These

constrain the minimum and maximum charging power $\underline{p}_{c,t}^{EV}$ and $\overline{p}_{c,t}^{EV}$ as well as minimum and maximum energy $\underline{e}_{c,t}$ and $\overline{e}_{c,t}$ for charging parks c

$$\underline{p}_{c,t}^{EV} \leq p_{c,t}^{EV} \leq \overline{p}_{c,t}^{EV} \qquad \forall t \in T, \quad c \in CP, \tag{4.15}$$

$$\underline{e}_{c,t} \leq e_{c,t} \leq \overline{e}_{c,t} \qquad \forall t \in T, \quad c \in CP, \tag{4.16}$$

$$e_{c,t} = \frac{1}{2} \cdot \left(\underline{e}_{c,t} + \overline{e}_{c,t}\right) \qquad \forall t \in \{0, t_{end}\}, \quad c \in CP, \tag{4.17}$$

$$e_{c,t} = e_{c,t-1} + \eta \cdot p_{c,t}^{EV} \cdot \Delta t \qquad \forall t \in T \setminus \{0\}, \quad c \in CP. \tag{4.18}$$

Equation (4.17) defines the state of charge (SOC) or energy level $e_{c,t}$ for the first and last time step to 50% of its capacity. Furthermore, the efficiency η during the entire charging process is assumed to be 90 % [76].

4.3.4 Heat Pumps & Thermal Storage

Modeling HPs with thermal energy storages (TESs) enables a shift of power consumption $p_{hp,t}^{HP}$ within a time frame while still meeting the residential heat demand $\dot{Q}_t^D$. The TES provides the flexibility. Our approach [53] allows the model to provide heat P_{th}^D by either direct HP use P_{th}^{HP} or thermal discharge of the TES P_{th}^{Stor} as shown in Figure 4.3.

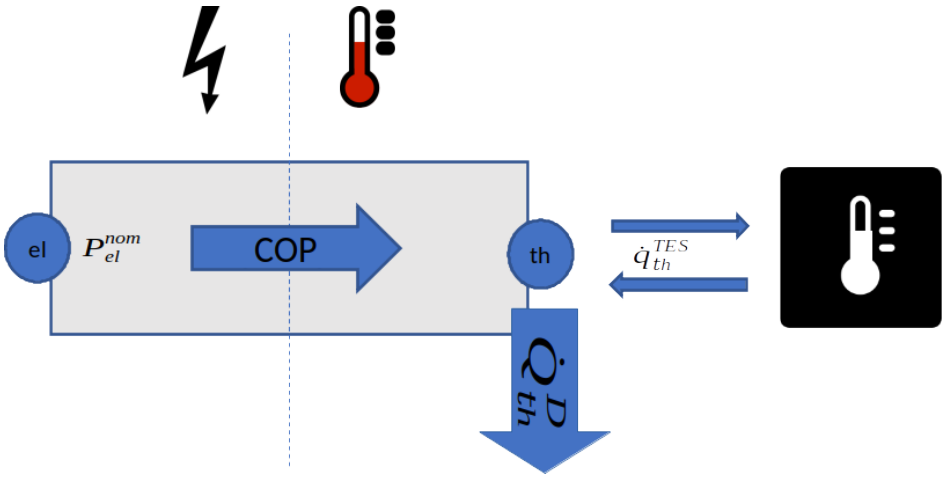

Figure 4.3: Implementation concept of a HPs with TES. A HP with a nominal electrical power P_{el}^{nom} transfers and amplifies heat to meet a thermal demand $\dot{Q}_{th}^{D}$. A TES is used to store heat $\dot{q}_{th}^{TES}$ temporarily.

The conversion factor between electrical P_{el}^{HP} and thermal power P_{th}^{HP} is defined by the coefficient of performance (COP) at time t. Equation (4.19) therefore, defines this relationship between the subcomponents. The thermal (dis-)charging $\dot{q}_{hp,t}^{TES}$ also directly relates to the state of energy of the TES $soe_{hp,t}^{TES}$ in Equation (4.22).

$$p_{h,t}^{HP} \cdot COP_{h,t} = \dot{Q}_t^D + \dot{q}_{h,t}^{TES} \qquad \forall t \in T, \quad h \in HP, \tag{4.19}$$

$$soe_{h,t}^{TES} = \eta_{th} \cdot soe_{h,t-1}^{TES} + \dot{q}_{h,t}^{TES} \cdot \Delta t \qquad \forall t \in T, \quad h \in HP \tag{4.20}$$

$$0 \leq \quad p_{h,t}^{HP} \quad \leq P_h^{nom} \qquad \forall t \in T, \quad h \in HP, \tag{4.21}$$

$$0 \leq soe_{h,t}^{TES} \leq C_h^{TES} \qquad \forall t \in T, \quad h \in HP, \tag{4.22}$$

$$soe_{h,-1}^{TES} = \frac{1}{2} \cdot C_h^{TES} \qquad \forall h \in HP, \tag{4.23}$$

$$soe_{h,t_{end}}^{TES} = \frac{1}{2} \cdot C_h^{TES} \qquad \forall h \in HP. \tag{4.24}$$

The thermal capacity $\dot{q}_{th}^{tes}$ is indirectly constrained by its two components. Which are either limited by the nominal power of the HP P_{hp}^{nom} or the thermal demand $\dot{Q}_t^D$. Regarding efficiency, we assume 4 % thermal loss per day [77], resulting in $\eta_{th} = 0.998\overline{3}$. Again, the state of energy (SOE) is fixed at first and last time step to 50% of its storage capacity.

4.4 Load balancing potential

Based on the concept of flexibility potential (introduced in Section 2.2.5), we derive the load balancing potential which the DG may offer to the transmission grid (TG) at the substation level. This is done by defining a flexibility interval, which we call ”flex-band”. The flex-band, is the range of possible states which all aggregated flexible units may assume. Hence, it can be used to constrain a dispatch optimization problem at the substation level. We apply four different objectives to determine the upper and lower bounds of the flex-bands for power consumption and energy level. Both flex-bands complement each other as they constrain the common solution space from different perspectives, grid, and component. For evaluation purposes, we define the load balancing potential (LBP) as metrics for the distance between upper $\overline{p}_{flex}$ and lower bound $\underline{p}_{flex}$ of the power consumption flex-band for all aggregated flexible units. It is an indicator that describes the maximum size of the interval. The greater the interval, the higher is the degree of freedom for the optimization of the component. This metric will be frequently used in the results evaluation.

$$\text{LBP(t)} = \overline{p}_{flex,t} - \underline{p}_{flex,t} \qquad \forall t \in T. \tag{4.25}$$

The optimizations are performed for the seven reinforcement scenarios described in Section 4.4.3 to evaluate the effects of reinforcement on LBP. These are again performed for each feeder separately and the results are subsequently aggregated.

4.4.1 Energy Level

The minimum and maximum aggregated cumulated energy of all flexible units are optimized to define the flexibility space from the component's perspective with the following equations:

$$\min_{p,q,\dot{q},e,soe,v} \sum_{t\in T} e_t^{cum} \qquad \forall t \in T, \tag{4.26}$$

$$\max_{p,q,\dot{q},e,soe,v} \sum_{t\in T} e_t^{cum} \qquad \forall t \in T, \tag{4.27}$$

$$e_t^{cum} = e_{t-1}^{cum} + \Big(\sum_{c\in CP} p_{c,t}^{EV} + \sum_{h\in HP} p_{h,t}^{HP} \Big) \cdot \Delta t \qquad \forall t \in T \setminus \{0\},\ c \in CP,\ h \in HP, \tag{4.28}$$

$$\tag{4.29}$$

The cumulated energy e_t^{cum} results from the previous time step value e_{t-1}^{cum} and the power consumed of all charging parks (CPs) $p_{c,t}^{EV}$ and HPs $p_{h,t}^{HP}$ in the current time frame Δt. The previous cumulated energy at the first time step is fixed to $e_{t=-1}^{cum} = 0$. The boundaries thus determined, represent the aggregated energy level if components maximize or minimize their power consumption, while staying within their constrained operating space (grid and storage capacity) but neglecting grid capacities. However, the grid model described in Section 4.3.2 is not included and only eqs. (4.15) to (4.24) are included.

4.4.2 Power

The minimum and maximum aggregated power of all flexible units are optimized to define the flexibility space from the grids' perspective with the following equations:

$$\min_{p,q,\dot{q},e,v} \quad \delta_{curt} \sum_{t\in T} \sum_{n\in N} p_{n,t}^{curt} + \delta_{power} \left(\sum_{c\in CP} p_{c,t}^{EV} + \sum_{h\in HP} p_{hp,t}^{HP} \right), \tag{4.30}$$

$$\max_{p,q,\dot{q},e,v} \quad -\delta_{curt} \sum_{t\in T} \sum_{n\in N} p_{n,t}^{curt} + \delta_{power} \left(\sum_{c\in CP} p_{c,t}^{EV} + \sum_{h\in HP} p_{hp,t}^{HP} \right), \tag{4.31}$$

$$\delta_{curt} = 10^{-2} \quad >> \quad \delta_{power} = 10^{-5}. \tag{4.32}$$

The active power of all BEV $p_{c,t}^{EV}$ and HP $p_{h,t}^{HP}$ is minimized or maximized, respectively, while the curtailment $p_{n,t}^{curt}$ at all nodes is minimized in both cases. Like before, we choose $\delta_{curt} = 10^{-2}$ and $\delta_{power} = 10^{-5}$ as weighting factors to make the component loading a minor criterion. The

curtailment at each node $p_{n,t}^{curt}$ is defined by the weighted sum of the active power curtailments, as in Section 4.3.1. Equation (4.5) is applied with the same fixed weighting factors to prefer curtailment of feed-in and BEVs over HPs and conventional load. Since we are not focusing on reactive power provisioning, we assume that the flexible loads do not draw any reactive power and that the reactive power curtailment of the load $q_{n,t}^{curt,l}$ and the feed-in $p_{n,t}^{curt,f}$ follow proportionally. However, in this case the variable $soe_{h,t}^{TES}$ describing the energy state for TESs is set unbounded, hence Equation (4.22) is excluded. Besides this, all of eqs. (4.6) to (4.24) are included.

4.4.3 Reinforcement Scenarios

To evaluate the flexibility potential of a minimally reinforced network and the effects of additional network expansion, the expansion measures must first be identified and applied. For this, we use the heuristic described in Section 2.2.4. However, several reinforcements may not succeed due to not converging power flow computations. To solve this, the basic reinforcement was enhanced by an iterative process using different approaches to gradually reinforce the network and fix any exceptions encountered. The basis reinforcement is the combined MV-LV one, which is tried first. If this fails, all the voltage levels are reinforced separately, starting with the MV level, adding the MV/LV transformers in a second iteration before reinforcing every LV grid on its own. Finally, a combined reinforcement iteration is started. All iterations are executed with the addition to reinforce the time steps with converging power flows first, appending another iteration for the not-yet converged time steps if any available. The process is depicted in Figure 4.4. After explaining the reinforcement procedure, the following describes the different expansion scenarios we use.

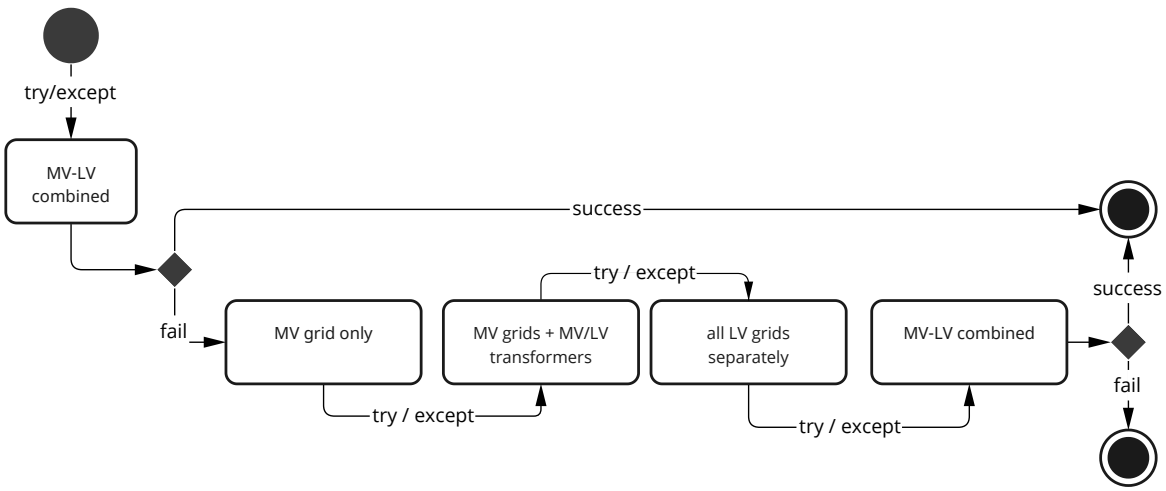

Figure 4.4: Description of the enhanced reinforcement process. MV-LV combined reinforces both voltage levels together. Catch convergence is an iterative process in which time steps with converging power flow are used first, triggering a second iteration for the not-yet converged ones.

Reference

As a reference scenario, the direct charging of BEVs at all locations and the HP operation without TES is used. This means that all BEVs are charged with max available charging capacity after arrival, assuming a charging efficiency $\eta = 0.9$. The thermal demand is directly served by the HPs without buffering heat using a TES. The electrical load of the heat pump is determined as follows:

$$P_t^{el} = \frac{P_t^{th}}{COP_t} \qquad \forall t \in T \tag{4.33}$$

For both components, functions are integrated in `eDisGo` to generate the active and reactive time-series. Again, a power factor of $cos(\phi) = 1$ is set. All other time-series stay unchanged. Based on these time-series, the steady-state is determined and grids are reinforced.

Minimal reinforcement

For a minimum reinforcement, we compute the optimal dispatch of flexible load units assuming that the curtailment and the load on the lines are minimized (Section 4.3.1). The resulting optimal dispatch time-series including the curtailed power for HPs and BEV are used to apply the reinforcement heuristic.

Partial Load

To evaluate the effect of the reinforcement on the flexibility potential, we also perform load-scaled reinforcements with an incremental increase of its effective flexible load $\mathrm{P}_{\mathrm{flex}}^{\mathrm{eff}}$. The implemented *worst-case analysis* of `eDisGo` for a load case scenario is used. The default factor-configuration of `eDisGo` is modified and the effective load of each CPs and HPs is increased from 20 % to 100 % of its nominal capacity $\mathrm{P}_{\mathrm{flex}}^{\mathrm{nom}}$ in 20 % steps for MV and LV.

$$P_{\mathrm{flex}}^{\mathrm{eff}} = i \cdot P_{\mathrm{flex}}^{\mathrm{nom}} \qquad \forall i \in \{0.2, 0.4, 0.6, 0.8, 1\},\ \mathrm{flex} \in \{CP, HP\}. \tag{4.34}$$

All inflexible load components are used at full power, but the injection of all generators is set to zero. This represents a hypothetical situation in which the entire load is drawn from the overlaid network. As a result, we expect the lines to be upgraded so that they can be used, in particular, for power input or output from the TG. Then, the steady-state with this configuration is determined by a power flow analysis and the necessary reinforcements are carried out. All partial load scenarios build on the reinforced grid of its predecessor, for example 60 % on 40 %. however, the 20 % scenario builds on the minimal line loading scenario.

5 Results & Discussion

This chapter is dedicated to presenting and discussing the findings and results of the analysis conducted on the distribution grids (DGs). The chapter is divided into five sections, each focusing on different aspects of the analysis. The first section (Section 5.1) introduces the identified periods used in the analysis. The second section (Section 5.2) compares the line loading optimized time series to the reference time series. The third section is dedicated to presenting the results for the reinforcement scenarios and is further divided into six parts. The first part (Section 5.3.1) compares the costs of the reinforcement scenarios, followed by the presentation and explanation of the determined flex-bands for a selected medium voltage grid district (MVGD) in the second part (Section 5.3.2). The third part (Section 5.3.3) compares the aggregated flex-bands for heat pumps (HPs) and battery electric vehicles (BEVs) and analyzes their behavior with increasing network reinforcement. The fourth part (Section 5.3.4) evaluates the load balancing potential (LBP) by their reinforcement scenarios, using one MVGD of each characteristic group (wind, photovoltaic (PV), load). The fifth part (Section 5.3.5) compares the performance of both observation periods. Finally, the effects of the reinforcement to the potential over the necessary costs are shown in the sixth part (Section 5.3.6). The chapter concludes with a discussion of the limitations of data and model in Section 5.4.

5.1 Observation Periods

Table 5.1 shows the selected time periods for the two research focuses (period selection described in Section 4.2.1) and each grid. The periods are colored corresponding to their seasons (spring in green, summer in orange, autumn in gray, winter in blue).

Table 5.1: Determined observation periods per grid for the respective focus.

	1690	1811	1056	176	177	2534
characteristic	Wind	Wind	PV	PV/Load	Load	Load
			Reinforcement			
start	12-04	04-26	05-01	05-05	01-20	12-05
end	12-10	05-02	05-07	05-11	01-26	12-11
			Flexibility potential			
start	01-26	11-14	12-13	06-09	04-19	04-19
end	02-01	11-20	12-19	06-15	04-25	04-25

It stands out that the period for reinforcement, which is selected by taking a week of high positive or negative mean value of the residual load, are solely in spring and winter. Whereas the periods to determine the flexibility potential, which is determined by the most balanced week of demand and supply, are more diverse. Another striking fact is that both load dominated grids (177, 2534) have the same timeframe selected, which is Easter and a public holiday. Therefore, demand is usually very low. In load dominated grids with a low renewable energy sources (RES), a low demand will lead to the most balanced situation of supply and demand. This can be seen in Figure 5.1 as the mean residual value is clearly lower in the flexibility potential period. A similar but opposite situation is shown for MVGD 1690 and 1811, where RES feed-in is dominated, and the most balanced situation is still a situation with high negative values. Only MVGD 1056 and 176 partially have a residual load of zero. However, the idea was to determine periods with free line capacity to determine a maximum flexibility potential, what is achieved in any of these cases.

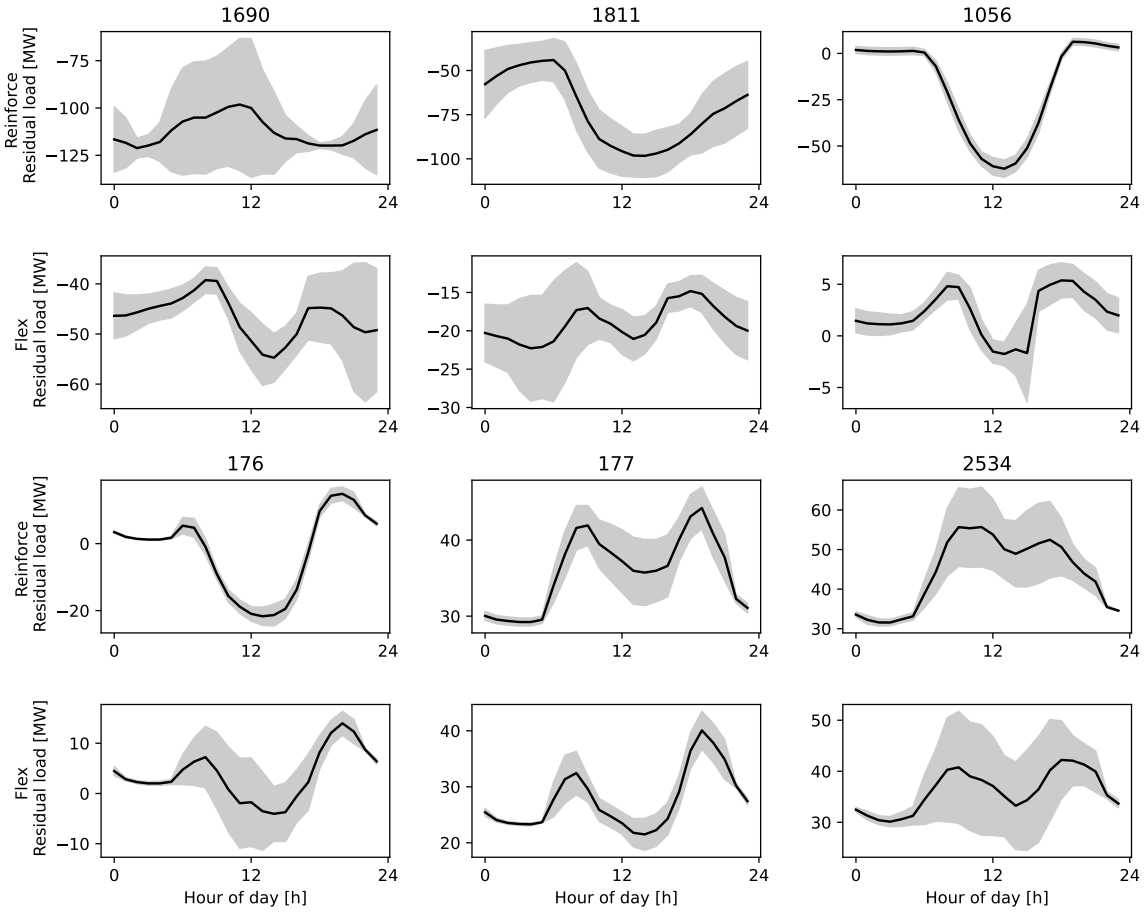

Figure 5.1: Hull curve of residual load values for 24 hours in each observation period (reinforcement and flexibility potential) and for every network. The mean value is depicted as a black line.

5.2 Optimized Dispatch

Figure 5.2 shows the results for the optimized dispatch of all flexible loads and compares them to the dispatch in the reference scenario as well as the grid residual load from the reference scenario for two selected networks. The loads of HPs and BEVs are aggregated values, with the lines representing the reference scenario and the filled areas representing the optimized dispatch. The dispatch of high power charging (HPC) and public charging parks are not included, as their consumption has not been optimized. The residual load scale is shown on the y-axis at the right-hand side. The negative or positive peaks indicate a high power exchange with the overlying grid level. It can be seen that both HP and BEV power consumption is shifted into two time periods on a daily basis compared to the reference scenario. There is both a noticeable peak at noon, when PV is fed in, and one at night, when the conventional load is lowest. The higher peak is always at times when the residual load is lowest. This pattern is more dominant for the HP share than for the BEV share. For HPs, there are even hours with almost no power consumption. The BEV power consumption, however, undergoes a peak shaving process, flattening its peaks to a more constant and steady shape, and decreasing during the late evening hours. Figure 5.2(a) illustrates MVGD 1811, Figure 5.2(b) MVGD 2534, representing a wind-dominated grid and a load-dominated grid, respectively. The fundamental difference is the value of the residual load, which defines the characteristics of the grid and the use of flexibility. In Figure 5.2(a) the HPs load, is shifted to midday when PV feed-in is high, and has its second but lower peak during the night where electricity demand from conventional loads is low. In both cases, line loading is minimized in total. During the day, local PV generation is used and during the night, free line capacities are used due to general low demand. In the load-dominated MVGD (Figure 5.2(b)), however, the HP peaks are shifted primarily into the early hours of the day, when the residual load is lowest, having its second, but not as dominant peak at midday. As can be seen in Table 5.2, the installed HPs and BEVs capacities, exceed the consumption in the period shown by more than a factor of 10. Here, it is clear, there is significant excess capacity, and it stands to reason that energy shifting would not be quite as successful with lower capacity.

Table 5.2: Installed peak loads, generation, and storage capacities as well as grid topology informations.

	1690	1811	1056	176	177	2534	unit
TES	61	81	51	133	100	46	MWh
HP	19	27	17	43	34	16	MW
BEV	27	32	28	71	67	37	MW
conventional load	13	14	12	36	45	65	MW
PV	38	23	99	60	23	17	MW
wind	138	125	8	6	0	0	MW
biomass	50	26	2	14	0	0	MW

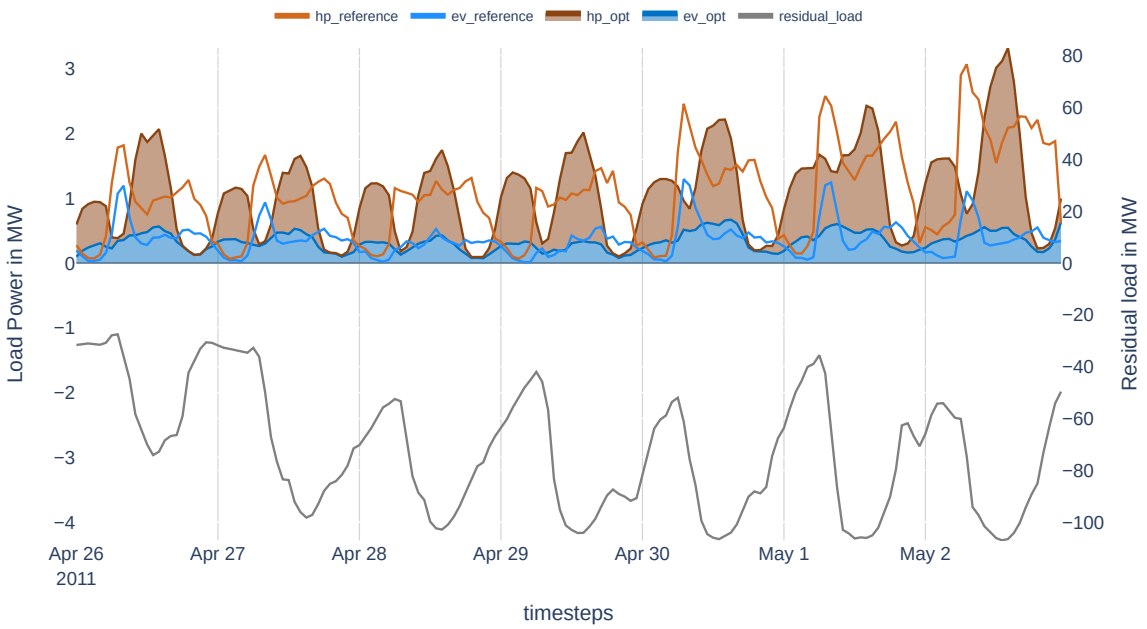

(a) Wind dominated MVGD 1811 during flexibility potential observation period

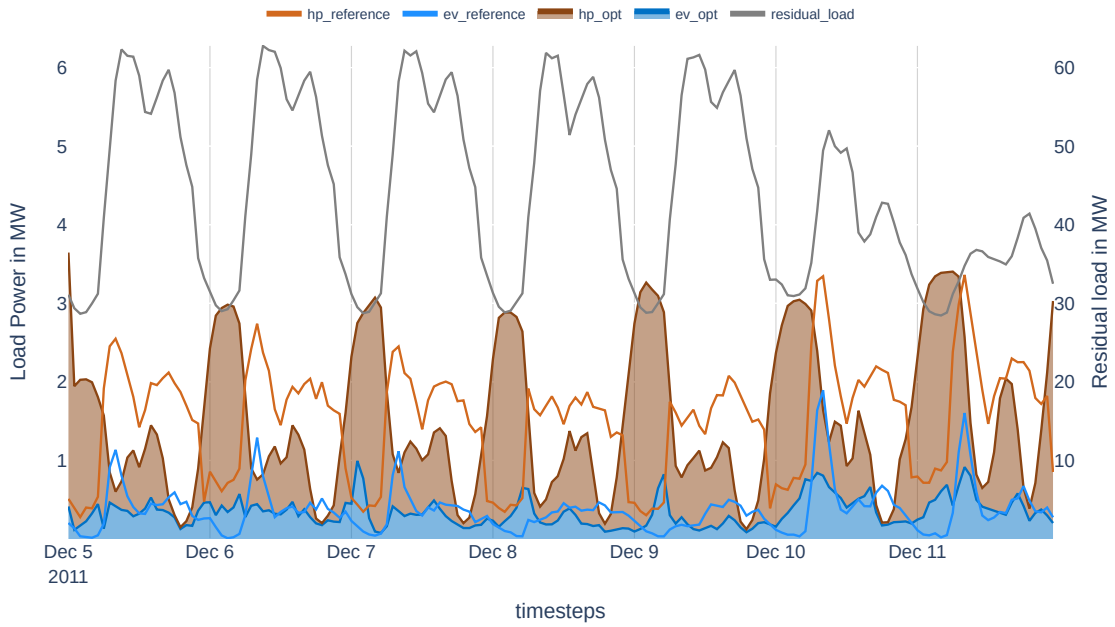

(b) Load dominated MVGD 2534 during flexibility potential observation period

Figure 5.2: Comparison of the dispatch of stacked BEV (blue) and HP (brown) in the minimal loading (filled area) and reference scenario (lines). The residual load on the right axis indicates the load or feed-in surplus in the reference scenario.

5.3 Reinforcement Scenarios

We applied seven reinforcement scenarios for each of the six networks, resulting in a total of 42 computed combination. Except for two scenarios of MVGD 177, which failed due to voltage issues, all were successful. The number of reinforcement iterations are shown in Table 5.3. By matching the iterations with the number of low voltage (LV) grids, we can see that MVGD 176 and 177 were reinforced with the enhanced algorithm in the reference and minimal loading scenarios.

Table 5.3: Successful reinforcement iterations per scenario. Values equal to one indicate a combined reinforcement of LV and medium voltage (MV) level, whereas values greater to one indicate that LV grids were reinforced separately.

	1690	1811	1056	176	177	2534
lv-grids total	179	381	130	196	110	56
reference	1	1	1	198	113	1
minimal	1	1	1	198	113	1
20% flex load	1	1	1	1	1	1
40% flex load	1	1	1	1	1	1
60% flex load	1	1	1	1	1	1
80% flex load	1	1	1	1	-	1
100% flex load	1	1	1	1	-	1

5.3.1 Costs

The reinforcement costs per voltage level for the network reinforcement scenarios described in Section 4.4.3 are shown in Figure 5.3 for each MVGD. All partial load scenarios are based on its predecessor and originate from the minimum line loading scenario. Therefore, the costs are interdependent and increase steadily from the minimal loading scenario upwards to the scenario 100 % flex load. Only the reference scenario is independent. In all networks, the reinforcement costs were reduced in the minimal line loading scenario compared to the reference scenario, as shown in Table 5.4.

Table 5.4: Total reinforcement costs of minimal line loading and reference reinforcement scenario for each grid in Mio €.

MVGD	1690	1811	1056	176	177	2534
minimal line loading	3.49	0.46	0.85	5.77	2.22	2.03
reference	3.72	0.67	1.63	8.50	5.01	2.41

The advantage of optimizing the use of BEV and HP over the direct charging pattern is particularly high in one of the load-dominated networks (177) and in the PV-dominated (1056), whereas in 2534, only slight reductions were realized. However, in three out of six

grids, costs in the reference scenario are lower than in the worst case scenario with 20 % partial load. One grid of each characteristic, wind (1811), PV (1056), and load-dominated (177), are represented. Although network 1811 is the most expensive (~35 Mio €) in its final stage of reinforcement, its minimal loading and 20 % scenario belong to the cheapest. From Table 5.2 we know about its high wind capacities. Therefore, the initial grid condition might already provided enough flexibility because of its necessity to export wind energy. However, there is a strikingly large increase in costs for the 40 % scenario in this and the 1056 grid. This is associated with a proportionally high share of reinforcement measures at the MV level. In both grids, multiple long distance MV-lines connecting LV-substations, were replaced and are responsible for the majority of the costs. MVGD as well has high PV capacities, which indicate, that sufficient line capacities were existent to transport energy to the transmission grid (TG). The PV dominated MVGD 176 is the only one with high expenditures at the LV level. Although, MVGD 176 and 177, had their LV levels reinforced separately, only 177 has that dominant LV costs. This might be connected to the high amount of BEV peak load. Although, also having high PV generation (Table 5.2), which is both installed at the LV-level, we have learned in Figure 5.2 that BEV load is not entirely shifted into the peaks but steadily spread over day and night. Gupta *et al.* claims, that PV leads to higher voltage violations and BEV to line overloading [48]. Both, happening during different times of the day, leads to more expensive reinforcements than in the others grids. In all other cases, the MV reinforcements make up the majority of the costs.

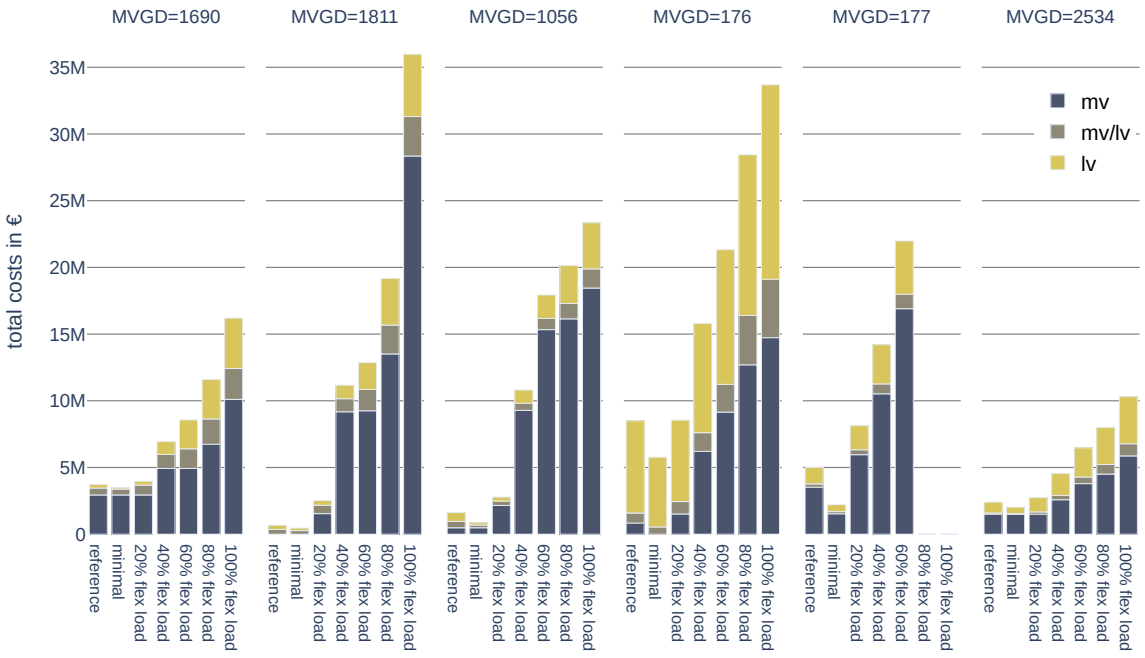

Figure 5.3: Absolute reinforcement costs for all scenarios and grids in €. The bars represent stacked costs of all measures summed per voltage level.

Figure 5.4 shows the additional reinforcement costs in each scenario as well as the share of the total costs when reinforced at last stage. The reference scenario is not included in this figure as it is a stand-alone scenario and not interdependent with the others. Each share of the pie represents the additional costs which occur. The summed shares of each grid accumulate to the value of the highest reinforcement level of the respective grid in Figure 5.3. It is necessary to mention, once again, that the 80 % and 100 % reinforcement scenarios of 177 did not succeed. Thus, the represented shares of total cost are significantly higher on this grid compared to the others. Throughout all MVGDs, the last reinforcement step is the most expensive one. This is particularly striking in the case of the feed-in dominated grids (1690, 1811). However, only in half of the cases, the minimal loading scenario is the cheapest. For the other half, the 20 % scenario is the one with the lowest costs. This comparison is somehow flawed, as the reinforcement approaches differ. In all other scenario steps, the load is increased by 20 %. In the minimum loading scenario, however, it is not possible to easily define to which level the load is increased as it is the result of an optimized dispatch. However, one can say reinforcement is happening and therefore, the difference between minimal loading and 20 % is in any case smaller than in the other scenarios, where the difference is defined by 20 % of the nominal power of all flexible loads. These results show that the expansion costs also differ proportionally to their scenarios. Since the networks were by purpose chosen to be heterogeneous, this is not an unexpected finding but emphasizes that characteristic groups should be examined again more closely.

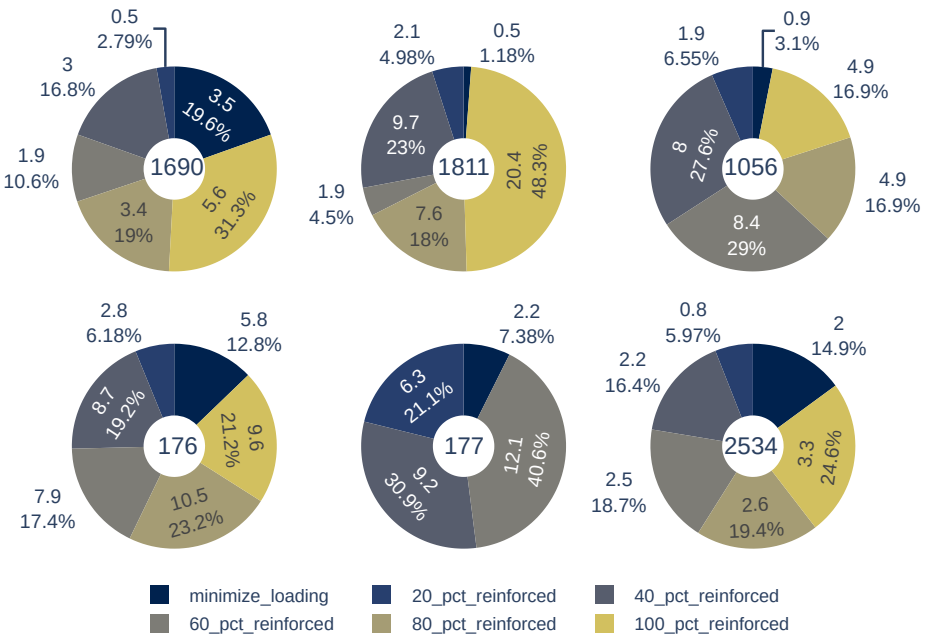

Figure 5.4: Additional reinforcement costs for each scenario in M€

5.3.2 Flex-bands

The optimizations described in Section 4.4 result in two time-series for power consumption and energy level, defining the upper and lower bounds of a flex-band (introduced in Section 2.2.5). These time-series were calculated for every scenario and network. The derived flex-bands describe the feasible operation space of all aggregated flexible loads under the condition of their common optimization over the whole timeframe. These are valid only in combination. Nevertheless, the bounds of the flexibility space are illustrated for the individual technologies in Figure 5.5. It should be noted that the bounds of the flex-bands for all scenarios, always remain within the defined absolute limits. To reduce complexity, the reference scenario is not shown as its bounds overlap with other scenarios. Figure 5.5(b) shows the flex-bands for all aggregated HPs and Figure 5.5(a) for all aggregated BEVs. We chose to show the plots of MVGD 1056, primarily for visualization purposes, as the results are the clearest to explain the dynamics and effects.

Power consumption (blue) and energy level (red) are shown together in both plots since they are interrelated (Section 2.2.5). The bounds of the flexibility potential are represented by lines. The figures also show the gradual increase in flexibility potential for each reinforcement scenario applied, indicated by filled areas between the lines. The teal lines indicate their theoretical upper and lower limits. Unlike the power consumption flex-bands, the energy level flex-bands do not vary with increasing reinforcement, as the grid model is not included in the optimization in this case. Therefore, only one pair of red lines is shown. Since the flex-bands are only valid together in any case, it is sufficient to show the constraints of the network in the power consumption. Also, one will notice that the graphs of HPs and BEVs look different. This is due to their different implementation approaches. BEVs are implemented as storage units which do not feed back into the system, so they can only increase their energy level. Therefore, the resulting time-series represent the cumulated energy level (red) and are shown in Figure 5.5(a). Furthermore, the aggregated power consumption is limited by the number of connected BEVs at the current time step, which results in a time-varying upper limit for the power consumption flex-band (teal). Therefore, the energy level and power consumption limits are defined by the BEV flex-bands (teal) used as input data (see Section 3.3). In contrast, the thermal energy storage (TES) of HPs are implemented as a typical storage that takes energy from the system and feeds it back. Thus, their energy level can increase and decrease. The upper limit (teal) of the power consumption flex-bands is similarly defined by the aggregated nominal power of all HP and the lower limit by zero. In Figure 5.5(a) and Figure 5.5(b) is shown that the potential for power consumption varies over time within the scenarios. The variation for BEV is much stronger than for HP, BEV with high peaks during the day. This counts for the upper and the lower bound. With each additional reinforcement level, an increase in flexibility potential for the power consumption can be seen for both technologies. The increase in range by the 40 % and 60 % flex load scenarios are much greater than by the others. In Figure 5.5(b), it is even the case that the 100 % flex load scenario has a little lower upper bound than the 80 % scenario. Therefore, the order in this plot was changed. In general,

the upper bound for the power consumption is shifted upwards with each scenario, but even in the 100% flex load scenario, the upper limit is not reached at all time steps. This counts for HPs and BEVs likewise, and for all grids. The reason for this again lies in our approach for the reinforcement. Since in the load-worst-case, no feed-in of RESs is considered. However, these require further capacities in the optimization. This does also apply to the lower bound, which defines the necessary power consumption to consume the least amount of power while having a stable grid. The magnitude of the lower bound is for both technologies very close to the zero line. Only in a few cases, there is a necessary power consumption. This does not apply for all grids and scenarios and will be further addressed in Section 5.3.3. Comparing the technologies, HPs provide a way more stable power consumption flex-band than BEVs. Also, its magnitude is much higher, than the one of BEVs. Although, the installed charging capacity of all charging parks (CPs) exceeds the one of all HPs, the limiting factor are the flex-bands of BEVs which actually define their maximum charging capacities. Since not all stations in a CP are always occupied, their potential cannot be fully utilized.

When looking at the energy level for BEVs, it is noticeable, that they almost entirely fit the limits. Only the first and last time steps differ, which is due to the fixed state of energy (SOE). The situation is entirely different for HPs. In the majority of time steps the bounds fit the limits, but big spikes occur for the upper and lower energy level bounds. This effect appears in all networks, but again to different extents. The origin lies in the interplay of the objective's formulation (Section 4.4.1), the TES and the time-series of the coefficient of performance (COP). As we minimize or maximize, the cumulated energy level over the whole period, the model tries to maximize or minimize the total amount of energy, using the COP and the TES in its favor. To yield the maximum, the TES is discharged in times of high COP and charged when COP is low. This way, the electricity consumption is increase due to the lower conversion factor. Additionally, early power consumption is rewarded as it propagates to subsequent time steps.

The results for the different networks vary widely within technologies. However, the general behavior of HPs and BEVs is transferable. This means that HPs offers a more constant flex-band in contrast to BEVs. This is mainly due to the fact that CPs themselves do not have a fixed capacity, as this depends on the number of vehicles to be charged. We will take a closer look at the already mentioned difference between the networks, in the following.

5.3.3 Flex-band Comparison

Now that we have gained an impression of the temporal course of the upper and lower bounds of the flexibility potential and have identified overlaps between the scenarios, we turn our attention to the distribution of the bound values. In Figure 5.6, aggregated values for HPs and BEVs are shown for each network. For each scenario, two boxplots depict the value distribution for the upper and lower bound. Only the four lowest reinforcement scenarios are shown, as the values of the higher ones are only slightly different from the upper and lower

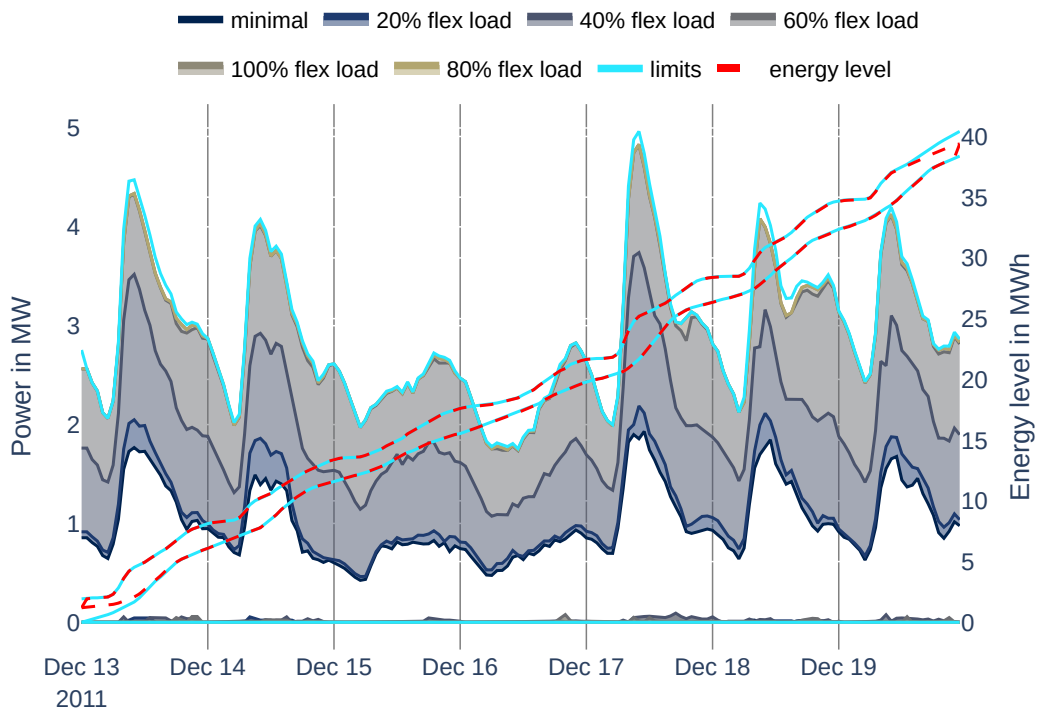

(a) Aggregated flex-bands for power and energy level of all BEV

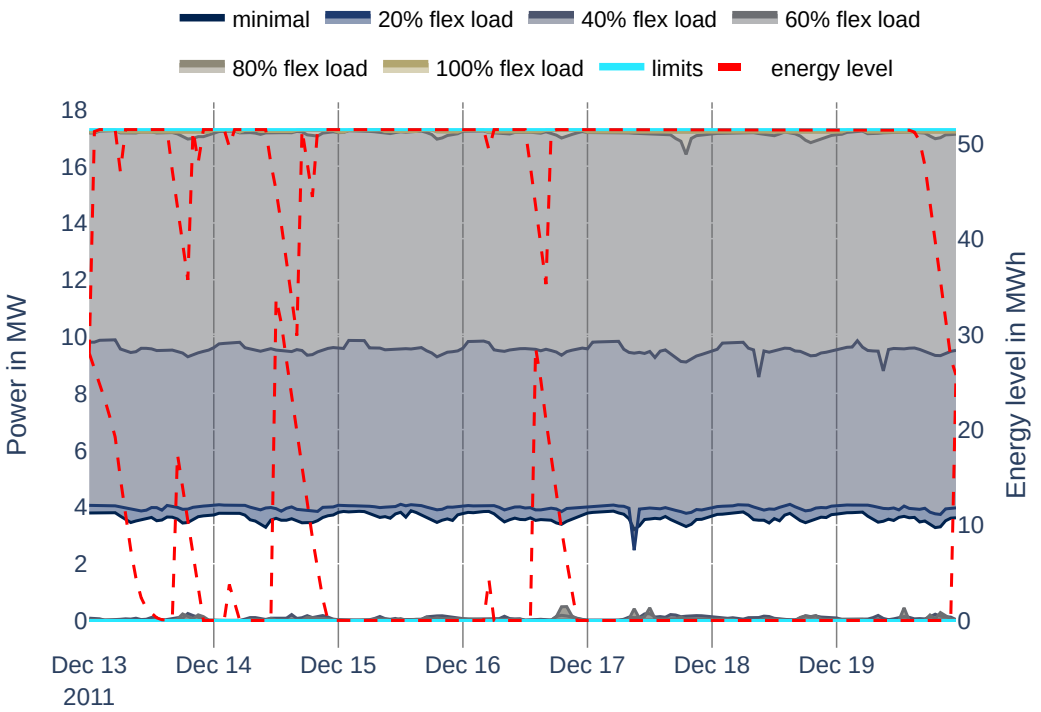

(b) Aggregated flex-bands for power and energy level of all HP

Figure 5.5: Representation of the determined upper and lower bounds describing the flex-bands for all scenarios of grid 1056. The minimum power potential is represented by not filled area. An increasing power potential, corresponding to the reinforcement scenarios, is indicated by the addition of colored areas at the top and bottom. The red lines describe the energy level boundaries.

limits and almost no overlaps with the other scenarios occur. It should be noted again, that the reference scenario is a stand-alone scenario and therefore no evolution to the other ones can be described, but its relation to the minimal scenario is to be considered. It is safe to say that the upper and lower bounds for the reference scenario are generally at the same level with the minimal scenario, but less narrow. Considering the fact that reinforcements have been in all networks more expensive and therefore probably more extensive, this appears reasonable. This is particularly noticeable for MVGD 176, 177, 2534, which are load-dominated networks (Figures 5.6(d) to 5.6(f)). For MVGD 176 and 177, this is consistent with their clearly higher reinforcement costs (Figure 5.3). The most narrow bounds are defined by the minimal load scenario of MVGD 1690. This strong wind dominated network, does not leave any space for flexibility as the bounds are so close, that they overlap in this representation. This needs further investigation, as the actual bounds should not overlap in any case. Looking at all the sequential scenarios, a general trend for a rising upper bound with increasing reinforcement is seen in MVGD 1690, 1056, 177, 2534 (Figures 5.6(a), 5.6(e) and 5.6(f)). At the same time, for some MVGDs, the lower bound is rising slightly and gets more scattered in the 40 % flex load scenario. This can be a result of a line splitting and the resulting change in load flows. In the reinforcement heuristic, line splitting is applied due to voltage issues. In some cases, the split line is connected directly to the HV-MV substation. As a result of this action, line flows may change, requiring flexible units to have a minimum necessary demand to stay within the grid constraints.

However, the grids seem to respond very differently to the reinforcements, focusing only at the four weakest scenarios. MVGD 1811 stands out as it has almost the same bounds for all depicted scenarios. It is able to offer a high potential already with the first reinforcement. This grid has high wind capacities, and is reinforced in a high wind period, therefore the lines are reinforced to transmit the energy into the TG. As the plots show a period of lower wind energy production, a lot of free line capacity is available for flexibility. It might even be possible, that the pre minimal loading grid condition offers sufficient potential as we have already seen, that the reinforcement costs were very low.

Although this is a good representation to analyze the bounds, it is difficult to evaluate the flexibility potential. The distance between the boxplots indicates the theoretical maximum flexibility potential, which is depicted in Figure 5.8 and further described in the following.

5.3.4 Load Balancing Potential

To evaluate the theoretical maximum flexibility potential at each time step, we calculate the distance from the lower to the upper bound, which we will call the ”LBP”. This key figure describes the maximum range which can be offered as possible flexible operating space at a certain time step. Whether two subsequent time steps can provide this range, always also depends on the potential of the energy levels.

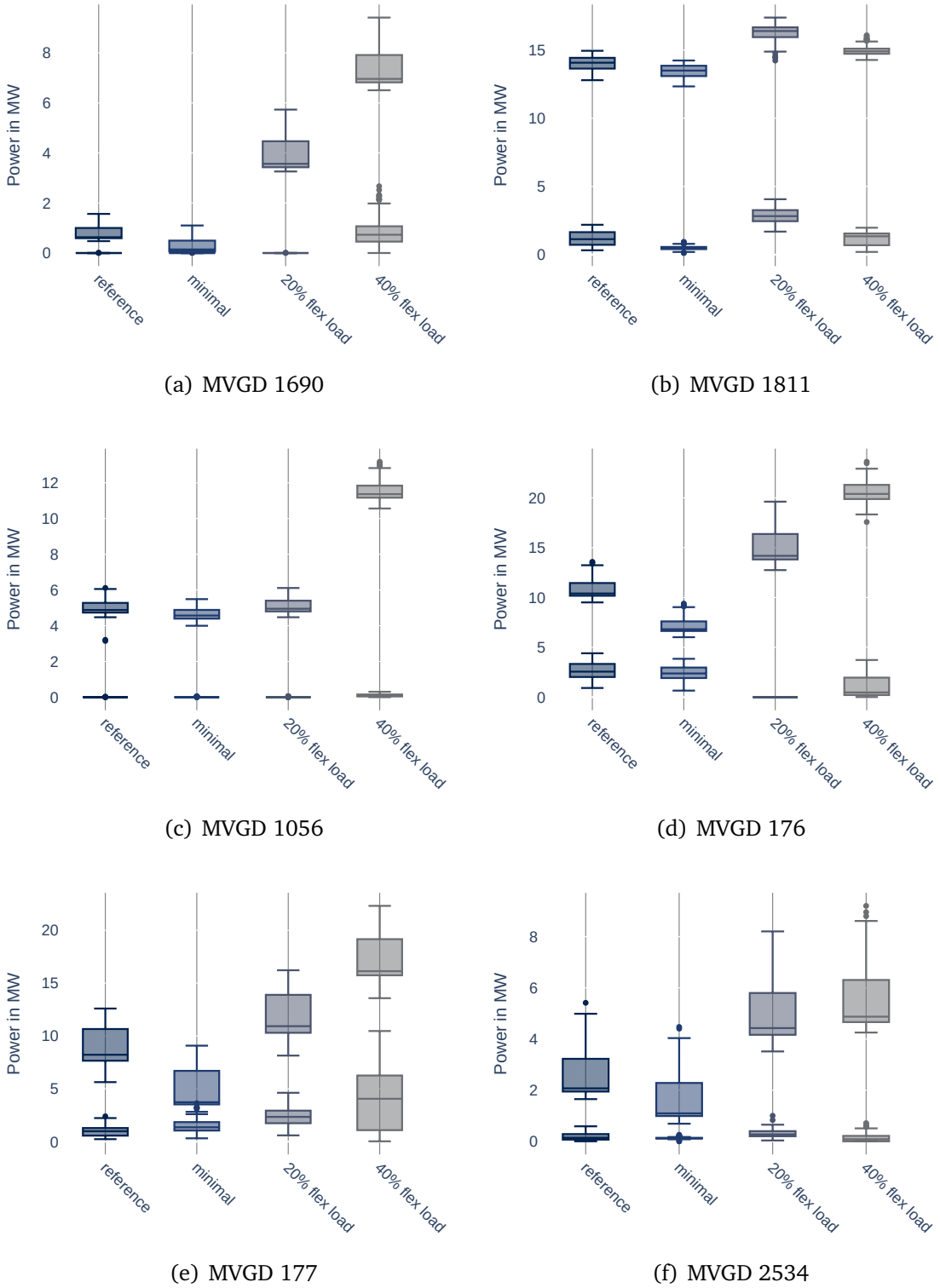

(a) MVGD 1690

(b) MVGD 1811

(c) MVGD 1056

(d) MVGD 176

(e) MVGD 177

(f) MVGD 2534

Figure 5.6: Distribution of the aggregated BEV and HP values for the upper and lower bounds of the flex-bands. Only the reinforcement scenarios with the most significant overlaps are depicted.

From now on, we use the aggregated time-series of HPs and BEVs. In Figure 5.7, the LBP is shown for one MVGD of each characteristic group. In order to compare the individual networks with one another, we calculate the ratio of the LBP and the peak load of all flexible units in the network. The results for each of them look differently, but all are far from reaching a ratio of one. This is because the CPs have a much higher installed capacity than their flex-band allows for optimization. This reflects reality in the sense that some charging points in a CP are idle. However, a direct correlation from the ratio of HP to BEV capacities is not possible because the limiting factors are the BEV flex-bands. In Figure 5.7(a), the potentials of the four weakest scenarios are of the same magnitude, but they are different from each other so that they overlap. We already recognized this in Figure 5.6(b) of Section 5.3.3. In the following 60 % scenario, a significant improvement in potential is achieved, with two more small improvements in the final scenarios. Further, with the 60 % scenario, some peaks appear more dominant. These can be attributed to BEVs as HPs provide a very stable flexibility. Figure 5.7(b) shows three major increases. The first is shared by the reference, minimal load, and 20 % scenarios, with some overlap that we already saw in Figure 5.6(c). The other improvements are achieved by the 40 % and 60 % flex load scenario. Again, the peaks can be attributed to BEVs. The load dominated MVGD in Figure 5.7(c), is the one with only minor increases during the weakest four scenarios. Significant increase takes place by the 60 % scenario, where it strongly approaches the maximum. Only negligible improvement can be realized in the last scenarios.

Generally, it can be stated that the potential keeps a very stable value over the week, with only slight fluctuations. This is due to the fact that mainly the HPs provides a stable potential compared to BEVs. However, the magnitude of BEVs are much smaller as seen in Figure 5.5. In Figures 5.7(a) and 5.7(b) the BEV peaks become more dominant with the stronger scenarios, whereas in Figure 5.7(c), these are present from the very beginning. This is explained by the fact, that the BEV capacity is more than twice as big as HP capacity which is the highest ratio for all grids.

Figure 5.8 describes the distribution of value for the LBP of all aggregated BEV and HP. All networks and scenarios are shown, besides the two unsuccessful ones of MVGD 177. In Section 5.3.3, we recognized the narrow bounds for the reference and minimal load scenario of MVGD 1690. Especially, for the minimal load scenario, it was striking. As we do not have negative values, the bounds do not overlap over time. Therefore, there is almost no potential to lift, but it is still a feasible solution. The data shows that by the 20 % scenario some potential can be provided, but an actual increase comes with the 60 % scenario.

So far, it has been noticeable that significant potential increase was made in the 60 % expansion scenario by most of the networks. The different potential gains in the weaker scenarios are attributed to the fact, that the reference, minimal load and 20 % flex load scenario all have different approaches but with certain grid characteristic, end up with a similar reinforcement effect. This can be seen in Figure 5.8(b), where the LBP overlaps as the values are of similar

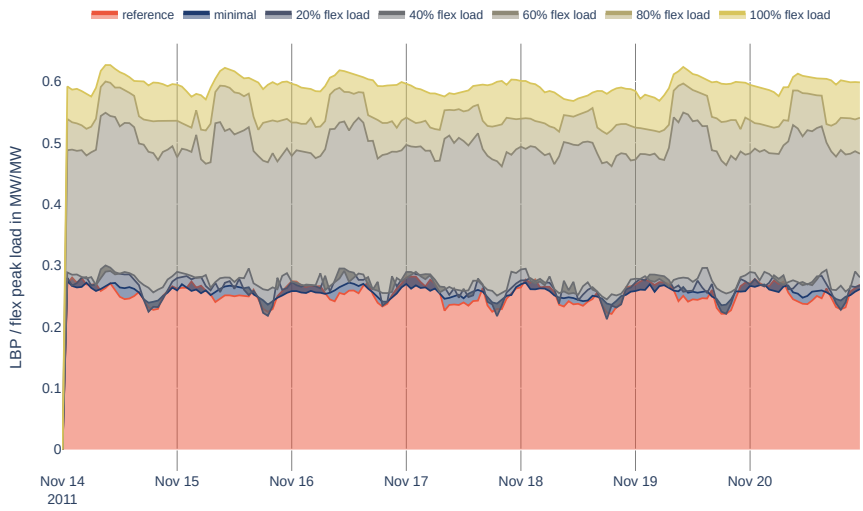

(a) MVGD 1811, wind dominated

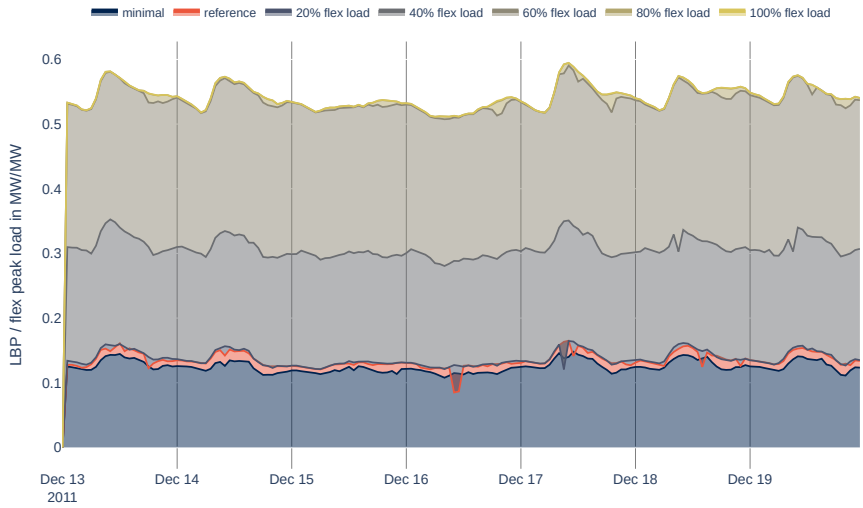

(b) MVGD 1056, PV dominated

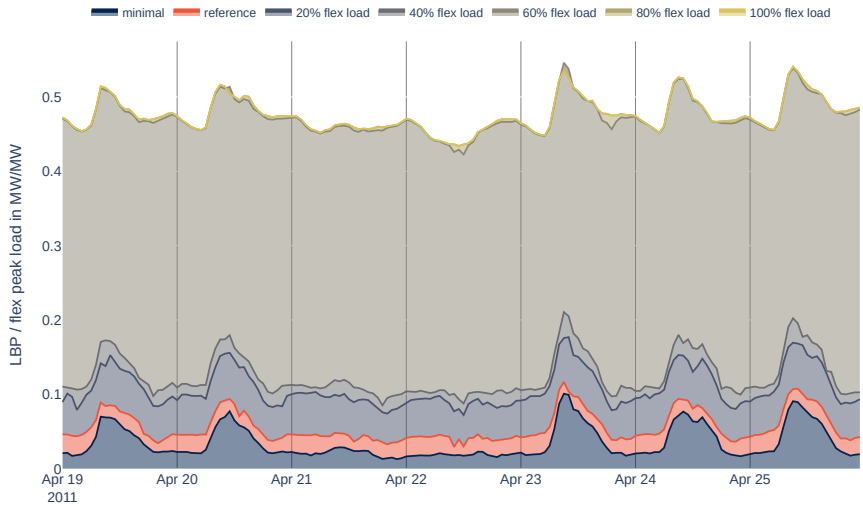

(c) MVGD 2534, load dominated

Figure 5.7: Progression of the ratio of load balancing potential to installed flexible peak load across the different scenarios. The filled areas show the increase of the ratio.

value. However, it seems that significant potential increases are to be achieved, with a load based reinforcement for the range of 40 % to 60 % of nominal flex load.

5.3.5 Observation Periods Comparison

To analyze the LBP, we focused on the period with the most balanced supply and demand ratio. However, in Figure 5.9 we want to compare the results of all considered time steps. The wind-dominated MVGD 1811 and the PV/load dominated MVGD 176 offer significantly higher potential in the flexibility period than in the reinforcement period. Although their generation and load characteristics are different, they have in common that they are the largest grids in terms of number of LV grids and total line length, as seen in Table 3.1. The networks are reinforced in both periods, which leaves a lot of free line capacity for flexibility during times when generation is not at maximum. This indicates that flexibility can only be provided temporarily. At least in the lower scenarios, where the deviations between the considered periods are most significant. Although the generation capacity in MVGD 1690, and the peak load of the flexible units is slightly lower (Table 5.2), additional reinforcements show an earlier effect in the 40 % scenario. The smallest grids in terms of number of LV grids and total line length are MVGDs 1056, 177 and 2534 (Figures 5.9(c), 5.9(e) and 5.9(f)). They perform better in the reinforcement period in the majority of scenarios. However, there are some differences between the scenarios in terms of variance and magnitude. The differences are of various kind, only the load dominated ones (Figures 5.9(e) and 5.9(f)) show similar values. This is because, even in the week we selected, supply and demand were far from balanced, placing a corresponding continuous load on the lines when they obtain power from the overlying grid and not locally. However, it is striking that the values for the 60 % are quite similar for all grids in both observation periods. This suggests that at this level of reinforcement, the effects of selecting a particular time period are negligible.

5.3.6 Cost Benefit Ratio

Finally, we want to draw a conclusion about the cost benefit ratio to provide distribution grid flexibility at the substation level. For this, we plot both LBP versus costs over installed peak load in Figure 5.10. This shows how much investment is needed to achieve a certain distribution grid flexibility. As the ”flexibility potential” period mostly performed better, we only include these values. Except for MVGD 1811, which provides early flexibility in the first stage of reinforcement, all other grids start with a low potential in the minimum load and reference scenario. However, to achieve high values no full reinforcement is needed. After the 60 % scenario almost no increase takes place for all networks. Hence, on a cost benefit basis this reinforcement is most profitable as further reinforcements basically only increase costs. MVGD 1056 is the only one that shows a somewhat linear increase from potential to relative cost until it approaches the maximum after the 60 % flex load scenario. Also, it belongs to

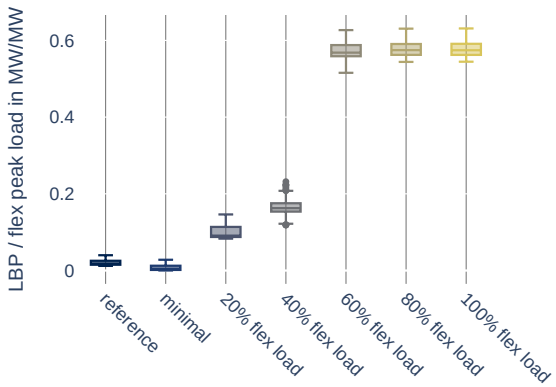

(a) MVGD 1690

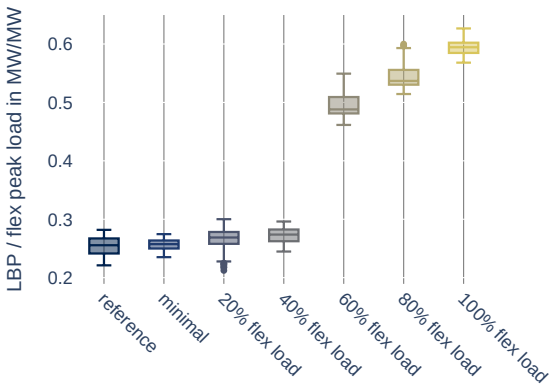

(b) MVGD 1811

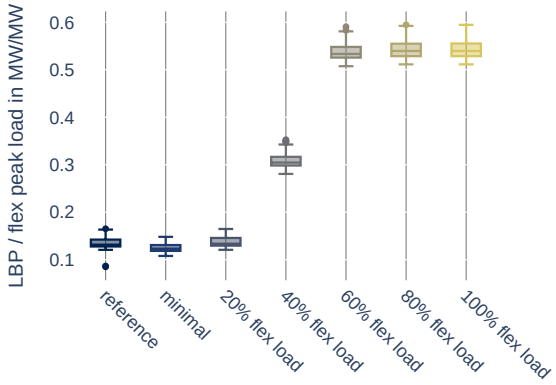

(c) MVGD 1056

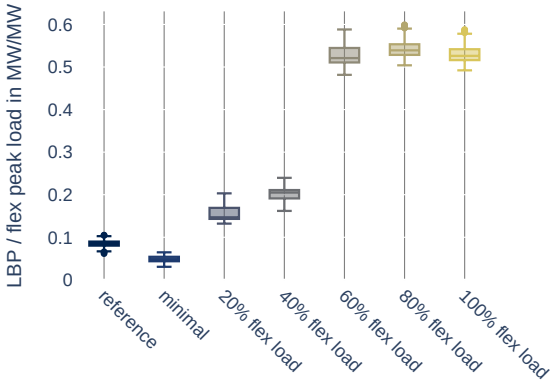

(d) MVGD 176

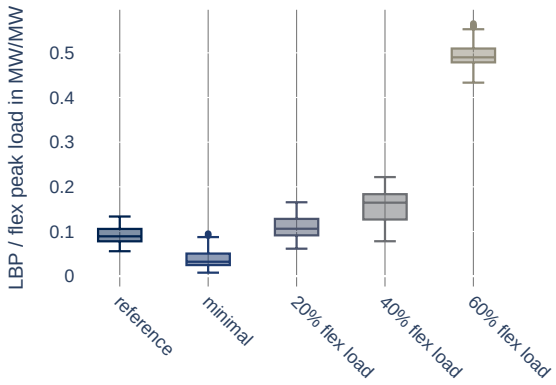

(e) MVGD 177

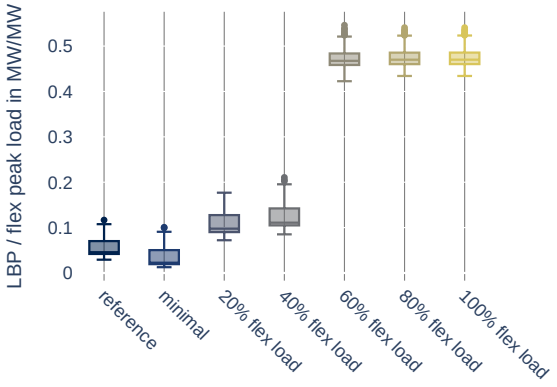

(f) MVGD 2534

Figure 5.8: Distribution of the ratio for aggregated load balancing potential (LBP) and installed peak load of all flexible units per scenario. The load balancing potential is the range between upper and lower bound of the flex-bands. Two scenarios for MVGD 177 are missing, as the reinforcements failed.

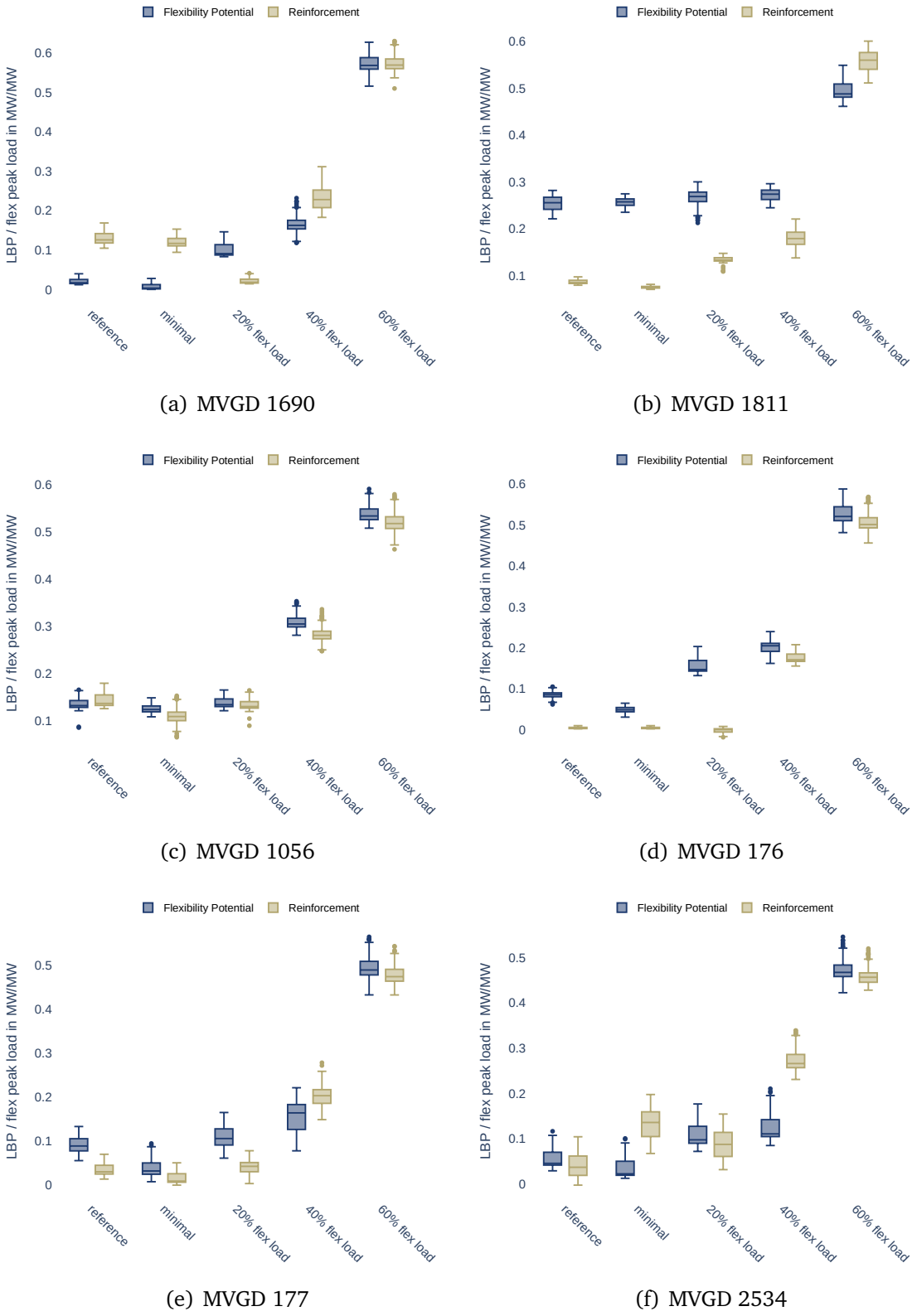

(a) MVGD 1690

(b) MVGD 1811

(c) MVGD 1056

(d) MVGD 176

(e) MVGD 177

(f) MVGD 2534

Figure 5.9: Comparison of the distribution of the load balancing potential values for two different observation periods of all scenarios up to 60 % flex load and each MVGD.

the most expensive ones. To achieve an LBP per flexible peak load of 0.5, close to 500 k€ per installed flexible peak load are necessary. In the other cases, an investment of 150-250k € per installed flexible peak load is sufficient.

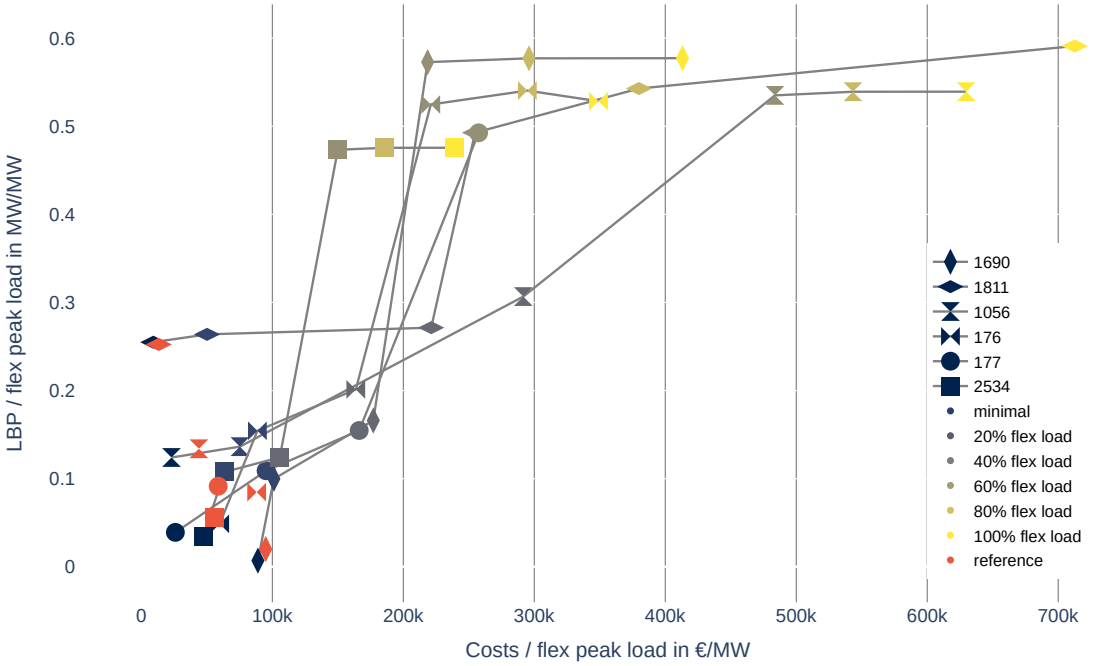

Figure 5.10: Trend of the load balancing potential per installed flexible peak load over the reinforcement costs per installed flexible peak load. The values are depicted for each scenario and MVGD. The lines follow the increasing reinforcement scenario. The reference scenario is stand-alone.

However, Figure 5.11 shows the reinforcement costs in relation to the costs of the minimal reinforcement costs. For half of the networks, the costs for the 60 % flex load scenario amount to two to three times the minimal reinforcement costs, which seem reasonable. For the rest, the costs amount to a factor of at least ten, up to 30. Investment with this cost factor seem unlikely. No patterns can be identified on the basis of the network characteristics.

Overall, the scatter plot provides useful insights into the trade-off between the benefits of reinforcement and the associated costs to achieve significant LBP in different networks. The cost of reinforcement relative to the minimum reinforcement shows again the additional investment that would be required. For half of the networks, cost and benefit seem promising.

5.4 Limitations

Finally, we want to discuss the limitations of our model and the data used. The data used has a huge impact on the results of our research. In the dispatch analysis, we already mentioned that load balancing of HP would probably not work as neatly if the capacity had not been oversized.

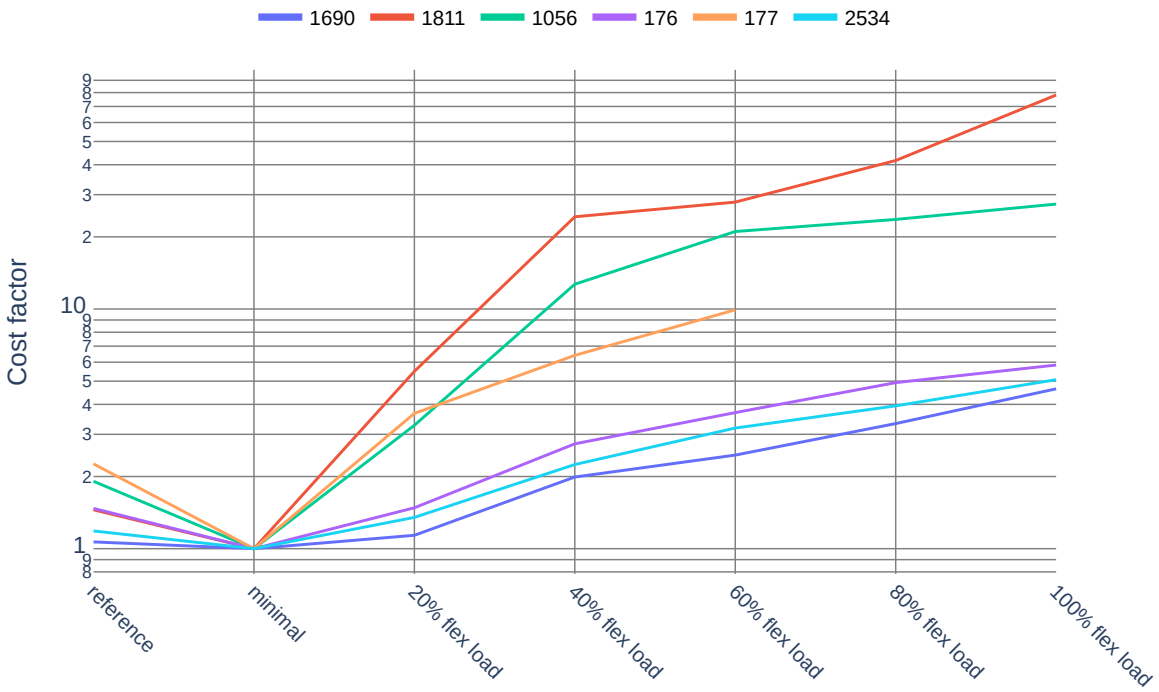

Figure 5.11: Reinforcement costs relative to the minimal reinforcement costs on a logarithmic scale.

This oversizing is due to the fact that the HPs should be able to cover a block of the six highest consecutive hours. Looking at a random heat profile of MVGD 1056 in Figure 5.12, one can see that there are only a few hours with really high demand. However, these hours influence the capacity sizing, especially since we add a flex factor to cover the potential blocking hours. Further, the TESs are then sized according to the HPs. This perpetuates the oversizing.

Kalz *et al.* find that the TES needs to cover five full-load hours for an annual optimal grid operation, which results in a volume of about $430\,\frac{\mathrm{l}}{\mathrm{kWh_{th}}}$ or only $170\,\frac{\mathrm{l}}{\mathrm{kWh_{th}}}$ if half of the operating hours should be grid optimal [22, p. 15]. Taking the median installed capacity in MVGD 1056 of $35\,\mathrm{kWh_{th}}$, with a temperature difference of $10\,\mathrm{K}$, we get a thermal storage volume of 3014 liter at an average maximum heat demand of $24.5\,\mathrm{kWh_{th}}$, resulting in a specific volume of $123\,\frac{\mathrm{l}}{\mathrm{kWh_{th}}}$. As we saw in Figure 5.12, only a few hours are of really high demand. If we were to use only the 99th quantile, we would only have an average maximum heat demand of $8\,\mathrm{kWh_{th}}$, resulting in a specific volume of $374\,\frac{\mathrm{l}}{\mathrm{kWh_{th}}}$. This shows that in this case, our heat storage assumptions are in a range close to those for a annual grid-optimized operation. This gave us the opportunity to show the potential of HP flexibility. However, it should be noted, that a specific volume of $25-50\,\frac{\mathrm{l}}{\mathrm{kWh_{th}}}$ is typically used for TES today [22, p.15].

The choice of model is also discussed. The study builds on a pre-existing model that uses the simplified dist-flow [41], which neglects the line losses during the calculation. This is done to linearize the model and reduce complexity. However, the line losses could be approximated ex

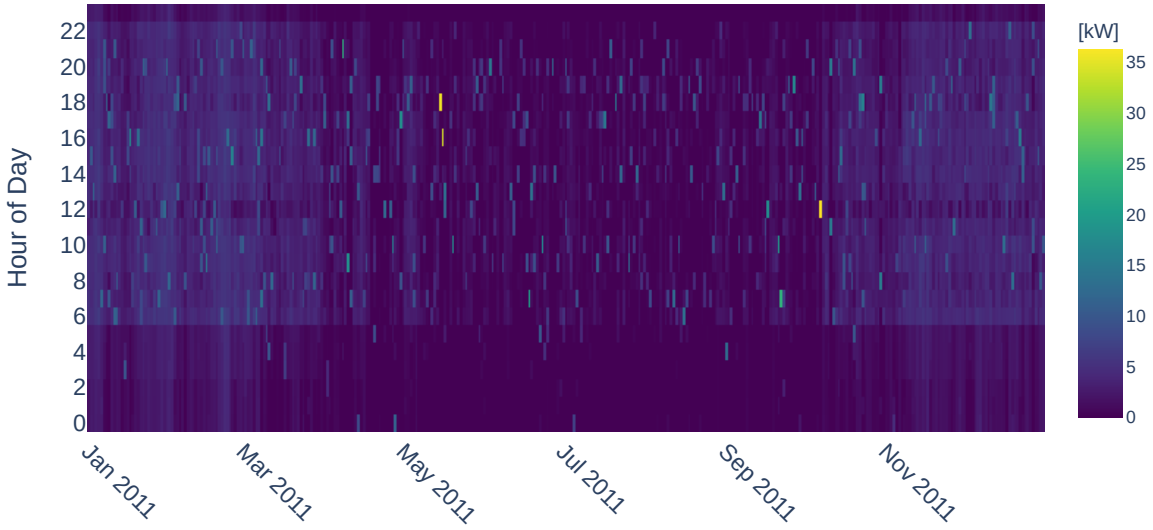

Figure 5.12: Heat demand of a random building in MVGD 1056.

post. This option has not yet been included in the model, but should be considered in further work. Especially in bigger DGs, the deviations can have a significant impact. In addition, the $(\mathcal{N}-1)$ criterion is not used. Its application is mandatory only at the MV level. However, since we were mainly focusing on the additional reinforcement, only to provide flexibility and not determine the actual dispatch, this assumption is reasonable. Thus, the $(\mathcal{N}-1)$ criterion should be considered when using the resulting flex-band as input for a dispatch optimization.

6 Conclusion & Outlook

In conclusion, this study explored the interplay between temporal and spatial flexibility in six DGs. Different scenarios were used to examine the impact of grid expansion on the provision of flexibility that is passed on to the transmission grid. For the scenario definition, we used the ego100 scenarios of the *open_eGo*[61] project for load and generation data and referred to the NEP C 2035 scenario[78] of the German network development plan (NDP) 2019 for the penetration of flexible demand units. First, a minimum required grid expansion was determined utilizing flexibility options such as BEVs and HPs with TES. The results showed that a significant amount of grid expansion costs could be saved using flexible loads compared to a reference scenario without flexibilization of the deployment. This amounted up to 1/3 of the total costs in the period under consideration. In addition, the study analyzed the potential to offer flexibility in the overlying grid. We determined flex-bands for the power-consumption and energy level of all aggregated flexible units by running multiple optimization models. These bands describe the distribution network flexibility of BEVs and HPs at the HV-MV substation. The evaluation with the LBP, representing the maximum potential, showed that, with a grid reinforcement oriented at the optimized flexibility dispatch, hardly any distribution grid flexibility could be offered. Moreover, various grid reinforcement scenarios with increased load demand for flexible units were defined. For this purpose, the load of all flexible consumers were increased in 20 % steps up to their nominal power and then, the grid reinforced. Again, the respective flex-bands were determined using the optimization models. The evaluation showed, that for most of the DGs, the relationship between network expansion and available flexibility is not linear. Furthermore, all grids reached values of their maximum potential after their 60 % flex load reinforcement scenario. The reinforcement costs reached values of 150-250k € per installed flexible peak load at this level. Only one grid had a linear relation and was about twice as expensive, with almost 500k € per installed flexible peak load. In relation to the minimum network expansion, it has been shown that for half of the networks, the costs amount to two to three times the minimum network expansion. For the rest, the costs amount to a factor of at least ten. Since the networks were very heterogeneous and the number was very small, no clear patterns could be detected. For this, the comparison of larger, more homogeneous groups would be helpful and could be the aim of further investigations. In addition, the total amount of flexibility that can be offered, depends heavily on the grid expansion, but also on the installed capacity of the flexible components. The data suggest that an expansion scenario based on an effective load of 40 %-60 % of the installed load for all flexible components would be the most effective. However, in our evaluation, we

referred exclusively to the network as a restrictive component. For further investigations, a sensitivity analysis with regard to installed capacities and penetration would be appropriate. Overall, we were able to show that optimized use of flexibility can save network expansion costs. Furthermore, our analysis has shown that with additional grid expansion, a significant flexibility potential could be made available for the overlying grid. The additional costs varied widely, but were only 200-300 % for half of the grids compared to the minimal reinforcement. Whether cost benefits are really profitable in the end should be determined in a further investigation on transmission grid level. For this purpose, the determined flex-bands can be used to constrain the aggregated flexibilities at the HV-MV station.

Bibliography

[1] E. European Union, *Commission Regulation (EU) 2017/1485 of 2 August 2017 establishing a guideline on electricity transmission system operation*, Aug. 2, 2017. [Online]. Available: https://eur-lex.europa.eu/eli/reg/2017/1485/2021-03-15 (visited on 04/02/2023).

[2] "Zukünftige Rolle des Verteilnetzbetreibers in der Energiewende," Mitnetz and E-Bridge, Eds., p. 7, 2017. [Online]. Available: https://www.bdew.de/media/documents/20160906_Studie-E-Bridge-MITNETZ-DSO2.0-Paper.pdf (visited on 07/29/2022).

[3] J. L. Ramirez-Mendiola, G. Mattioli, J. Anable, and J. Torriti, "I'm coming home (to charge): The relation between commuting practices and peak energy demand in the United Kingdom," *Energy Research & Social Science*, vol. 88, p. 102 502, Jun. 1, 2022, ISSN: 2214-6296. DOI: 10.1016/j.erss.2022.102502. [Online]. Available: https://www.sciencedirect.com/science/article/pii/S221462962200010X (visited on 04/04/2023).

[4] F. D'Ettorre, M. Banaei, R. Ebrahimy, *et al.*, "Exploiting demand-side flexibility: State-of-the-art, open issues and social perspective," *Renewable & Sustainable Energy Reviews*, vol. 165, no. 112605, Sep. 2022, ISSN: 1364-0321. DOI: 10.1016/j.rser.2022.112605.

[5] "eGon - Open, inter-grid-level and cross-sectoral planning instrument for the optimal use and expansion of the electrical grid and flexibility options in Germany." (Jan. 2, 2020), [Online]. Available: https://ego-n.org/ (visited on 01/27/2023).

[6] J. Amme, G. Pleßmann, J. Bühler, L. Hülk, E. Kötter, and P. Schwaegerl, "The eGo grid model: An open-source and open-data based synthetic medium-voltage grid model for distribution power supply systems," *Journal of Physics: Conference Series*, vol. 977, p. 012 007, Feb. 2018, ISSN: 1742-6596. DOI: 10.1088/1742-6596/977/1/012007. [Online]. Available: https://doi.org/10.1088/1742-6596/977/1/012007 (visited on 09/26/2022).

[7] open_eGo-Team. "eDisGo Documentation." (), [Online]. Available: https://edisgo.readthedocs.io/en/dev/ (visited on 03/20/2023).

[8] U. Maier, "Verteilnetzausbau für die Energiewende - Elektromobilität im Fokus," Agora Energiewende, Agora Verkehrswende, Aug. 2019, p. 114. [Online]. Available: https://www.agora-energiewende.de/fileadmin/Projekte/2018/Netzausbau_Elektromobilitaet/Agora-Verkehrswende_Agora-Energiewende_EV-Grid_WEB.pdf (visited on 10/09/2022).

[9] DIN e.V., "CENELEC-Normspannungen," pat., Apr. 2012. [Online]. Available: https://www.beuth.de/de/norm/din-en-60038/148204325 (visited on 02/26/2023).

[10] VDE FNN. "Das Stromnetz in Deutschland: Was es kann und wie es funktioniert," Backbone. (Apr. 29, 2022), [Online]. Available: https://backbone.vde.com/das-stromnetz-was-es-kann-wie-es-funktioniert/ (visited on 02/25/2023).

[11] L. Verheggen, R. Ferdinand, and A. Moser, "Planning of low voltage networks considering distributed generation and geographical constraints," in *2016 IEEE International Energy Conference (ENERGYCON)*, Apr. 2016, pp. 1–6. DOI: 10.1109/ENERGYCON.2016.7514042.

[12] K. Heuck, K.-D. Dettmann, and D. Schulz, *Elektrische Energieversorgung: Erzeugung, Übertragung und Verteilung elektrischer Energie für Studium und Praxis*, 8., überarb. und aktualisierte Aufl, ser. Studium. Wiesbaden: Vieweg + Teubner, 2010, 783 pp., ISBN: 978-3-8348-0736-6.

[13] A. J. Schwab, "Verteilung elektrischer Energie," in *Elektroenergiesysteme: Erzeugung, Übertragung und Verteilung elektrischer Energie*, A. J. Schwab, Ed., Berlin, Heidelberg: Springer, 2017, pp. 545–588, ISBN: 978-3-662-55316-9. DOI: 10.1007/978-3-662-55316-9_11. [Online]. Available: https://doi.org/10.1007/978-3-662-55316-9_11 (visited on 02/25/2023).

[14] B. BNetzA. "Aktuelle Strommarktdaten." (), [Online]. Available: https://www.bundesnetzagentur.de/DE/Fachthemen/ElektrizitaetundGas/HandelundVertrieb/SMARD/Aktuelles/start.html;jsessionid=1E14A30F05C0F5EEF87DF986468338CC#[Anker] (visited on 02/25/2023).

[15] B. BNetzA and B. BKartA, "Monitoringbericht 2021," Bundesnetzagentur für Elektrizität, Gas, Bundeskartellamt Telekommunikation, Post und Eisenbahnen und Bundeskartellamt, 2022, p. 540. [Online]. Available: https://www.bundesnetzagentur.de/SharedDocs/Mediathek/Monitoringberichte/Monitoringbericht_Energie2021.pdf;jsessionid=76ACB94FC445A77B2CF03E96FAB9EE__blob=publicationFile&v=7 (visited on 10/17/2022).

[16] J. Henkel, "Redispatch and Curtailment to Manage Grid Integration," Apr. 11, 2019. [Online]. Available: https://www.agora-energiewende.de/fileadmin/

Projekte/2019/VAs_sonstige/Grids_ThinkTank-Workshop/02_Johannes_Henkel_50Hertz_Grid-Workshop_11042019.pdf (visited on 10/10/2022).

[17] bbh, "Verteilnetzbetreiber 2030," becker büttner held, May 2018. [Online]. Available: https://www.die-bbh-gruppe.de/fileadmin/user_upload/Aktuelles/Studien/Studie_VNB_2030.pdf (visited on 02/25/2023).

[18] T. Ackermann and V. Knyazkin, "Interaction between distributed generation and the distribution network: Operation aspects," in *IEEE/PES Transmission and Distribution Conference and Exhibition*, vol. 2, Oct. 2002, 1357–1362 vol.2. DOI: 10.1109/TDC.2002.1177677.

[19] H. Algarvio, A. Couto, D. de São José, *et al.*, "Temporal flexibility options in electricity market simulation models," Berichtsreihe, Aug. 31, 2021. [Online]. Available: https://elib.dlr.de/147026/ (visited on 10/09/2022).

[20] L. Maeyaert, L. Vandevelde, and T. Döring, "Battery Storage for Ancillary Services in Smart Distribution Grids," *Journal of Energy Storage*, vol. 30, p. 101 524, Aug. 1, 2020, ISSN: 2352-152X. DOI: 10.1016/j.est.2020.101524. [Online]. Available: https://www.sciencedirect.com/science/article/pii/S2352152X19310898 (visited on 03/05/2023).

[21] frontier economics, "Beitrag von Flexibilitäten im Verteilnetz zur Senkung der Redispatchkosten in Deutschland," Jul. 2017. [Online]. Available: https://www.bdew.de/media/documents/20170809_Studie-Redispatchkosten.pdf (visited on 02/26/2023).

[22] D. Kalz, K. Klein, and A. Palzer, "Netzdienliche Gebäude und Quartiere. Gebäude entlasten Stromnetze," BINE Informationsdienst, FIZ Karlsruhe, Bonn, 2018, p. 24. [Online]. Available: https://www.baufachinformation.de/netzdienliche-gebaeude-und-quartiere/bu/2018079000385 (visited on 03/10/2023).

[23] J. Ramsebner, R. Haas, A. Ajanovic, and M. Wietschel, "The sector coupling concept: A critical review," *WIREs Energy and Environment*, vol. 10, no. 4, e396, 2021, ISSN: 2041-840X. DOI: 10.1002/wene.396. [Online]. Available: https://onlinelibrary.wiley.com/doi/abs/10.1002/wene.396 (visited on 03/06/2023).

[24] P. S. R. Murty, "Chapter 19 - Load Flow Analysis," in *Electrical Power Systems*, P. S. R. Murty, Ed., Boston: Butterworth-Heinemann, Jan. 1, 2017, pp. 527–587, ISBN: 978-0-08-101124-9. DOI: 10.1016/B978-0-08-101124-9.00019-X. [Online]. Available: https://www.sciencedirect.com/science/article/pii/B978008101124900019X (visited on 02/24/2023).

[25] A. Mary, B. Cain, and R. O'Neill, "History of optimal power flow and formulations," *Fed. Energy Regul. Comm.*, vol. 1, pp. 1–36, Jan. 2012.

[26] J. D. Glover, M. S. Sarma, and T. Overbye, *Power System Analysis and Design*. Cengage Learning, Jan. 3, 2011, 850 pp., ISBN: 978-1-111-42577-7.

[27] J. Grainger and W. Stevenson, *Power System Analysis*, ser. Electrical Engineering Series. McGraw-Hill, 1994, ISBN: 978-0-07-113338-8. [Online]. Available: https://books.google.de/books?id=a1OzQgAACAAJ.

[28] S. Chatzivasileiadis. "Lecture Notes on Optimal Power Flow (OPF)." arXiv: arXiv:1811.00943. (Nov. 2, 2018), [Online]. Available: http://arxiv.org/abs/1811.00943 (visited on 09/26/2022), preprint.

[29] D. K. Molzahn and I. A. Hiskens, "A Survey of Relaxations and Approximations of the Power Flow Equations," *Foundations and Trends® in Electric Energy Systems*, vol. 4, no. 1-2, pp. 1–221, 2019, ISSN: 2332-6557, 2332-6565. DOI: 10.1561/3100000012. [Online]. Available: http://www.nowpublishers.com/article/Details/EES-012 (visited on 02/20/2023).

[30] T. Brown, J. Hörsch, and D. Schlachtberger, "PyPSA: Python for Power System Analysis," *Journal of Open Research Software*, vol. 6, no. 1, p. 4, 1 Jan. 16, 2018, ISSN: 2049-9647. DOI: 10.5334/jors.188. [Online]. Available: http://openresearchsoftware.metajnl.com/article/10.5334/jors.188/ (visited on 02/15/2023).

[31] W. F. Tinney and C. E. Hart, "Power Flow Solution by Newton's Method," *IEEE Transactions on Power Apparatus and Systems*, vol. PAS-86, no. 11, pp. 1449–1460, Nov. 1967, ISSN: 0018-9510. DOI: 10.1109/TPAS.1967.291823.

[32] C. Coffrin and L. Roald. "Convex Relaxations in Power System Optimization: A Brief Introduction." arXiv: arXiv:1807.07227. (Jul. 18, 2018), [Online]. Available: http://arxiv.org/abs/1807.07227 (visited on 02/13/2023), preprint.

[33] D. Bienstock and A. Verma. "Strong NP-hardness of AC power flows feasibility." arXiv: arXiv:1512.07315. (Apr. 9, 2019), [Online]. Available: http://arxiv.org/abs/1512.07315 (visited on 02/22/2023), preprint.

[34] K. Lehmann, A. Grastien, and P. Van Hentenryck, "AC-Feasibility on Tree Networks is NP-Hard," *IEEE Transactions on Power Systems*, vol. 31, no. 1, pp. 798–801, Jan. 2016, ISSN: 1558-0679. DOI: 10.1109/TPWRS.2015.2407363.

[35] M. Baran and F. Wu, "Optimal capacitor placement on radial distribution systems," *IEEE Transactions on Power Delivery*, vol. 4, no. 1, pp. 725–734, Jan. 1989, ISSN: 1937-4208. DOI: 10.1109/61.19265.

[36] M. Baran and F. Wu, "Optimal sizing of capacitors placed on a radial distribution system," *IEEE Transactions on Power Delivery*, vol. 4, no. 1, pp. 735–743, Jan. 1989, ISSN: 1937-4208. DOI: 10.1109/61.19266.

[37] B. Subhonmesh, S. H. Low, and K. M. Chandy, "Equivalence of branch flow and bus injection models," in *2012 50th Annual Allerton Conference on Communication, Control, and Computing (Allerton)*, Oct. 2012, pp. 1893–1899. DOI: 10.1109/Allerton.2012.6483453.

[38] S. H. Low, "Convex Relaxation of Optimal Power Flow—Part I: Formulations and Equivalence," *IEEE Transactions on Control of Network Systems*, vol. 1, no. 1, pp. 15–27, Mar. 2014, ISSN: 2325-5870. DOI: 10.1109/TCNS.2014.2309732. [Online]. Available: http://ieeexplore.ieee.org/document/6756976/ (visited on 02/16/2023).

[39] N. Li, L. Chen, and S. H. Low, "Exact convex relaxation of OPF for radial networks using branch flow model," in *2012 IEEE Third International Conference on Smart Grid Communications (SmartGridComm)*, Nov. 2012, pp. 7–12. DOI: 10.1109/SmartGridComm.2012.6485951.

[40] M. Farivar and S. H. Low, "Branch Flow Model: Relaxations and Convexification—Part I," *IEEE Transactions on Power Systems*, vol. 28, no. 3, pp. 2554–2564, Aug. 2013, ISSN: 1558-0679. DOI: 10.1109/TPWRS.2013.2255317.

[41] M. Baran and F. Wu, "Network reconfiguration in distribution systems for loss reduction and load balancing," *IEEE Transactions on Power Delivery*, vol. 4, no. 2, pp. 1401–1407, Apr. 1989, ISSN: 1937-4208. DOI: 10.1109/61.25627.

[42] S. Lumbreras and A. Ramos, "The new challenges to transmission expansion planning. Survey of recent practice and literature review," *Electric Power Systems Research*, vol. 134, pp. 19–29, May 1, 2016, ISSN: 0378-7796. DOI: 10.1016/j.epsr.2015.10.013. [Online]. Available: https://www.sciencedirect.com/science/article/pii/S0378779615003090 (visited on 04/03/2023).

[43] H. Haghighat and B. Zeng, "Security-constrained robust dynamic power system planning with discrete recourse," *Electric Power Systems Research*, vol. 214, p. 108 858, Jan. 1, 2023, ISSN: 0378-7796. DOI: 10.1016/j.epsr.2022.108858. [Online]. Available: https://www.sciencedirect.com/science/article/pii/S0378779622009117 (visited on 04/03/2023).

[44] C. Rehtanz, M. Greve, U. Häger, and Z. Hagemann, "Verteilnetzstudie für das Land Baden-Württemberg," Technische Universität Dortmund ie3 Institut für Energiesysteme, Energieeffizienz und Energiewirtschaft, Ministerium für Umwelt, Klima und Energiewirtschaft Baden-Württemberg, Dortmund, 2017.

[45] U. P. Müller, B. Schachler, M. Scharf, *et al.*, "Integrated Techno-Economic Power System Planning of Transmission and Distribution Grids," *Energies*, vol. 12, no. 11, p. 2091, 11 Jan. 2019, ISSN: 1996-1073. DOI: 10.3390/en12112091. [Online]. Available: https://www.mdpi.com/1996-1073/12/11/2091 (visited on 03/22/2023).

[46] dena, "Ausbau- und Innovationsbedarf der Stromverteilnetze in Deutschland bis 2030," Dec. 11, 2012. [Online]. Available: https://www.dena.de/fileadmin/dena/Dokumente/Pdf/9100_dena-Verteilnetzstudie_Abschlussbericht.pdf (visited on 08/01/2022).

[47] R. D'hulst, W. Labeeuw, B. Beusen, S. Claessens, G. Deconinck, and K. Vanthournout, "Demand response flexibility and flexibility potential of residential smart appliances: Experiences from large pilot test in Belgium," *Applied Energy*, vol. 155, pp. 79–90, Oct. 1, 2015, ISSN: 0306-2619. DOI: 10.1016/j.apenergy.2015.05.101. [Online]. Available: https://www.sciencedirect.com/science/article/pii/S0306261915007345 (visited on 03/06/2023).

[48] R. Gupta, A. Pena-Bello, K. N. Streicher, *et al.*, "Spatial analysis of distribution grid capacity and costs to enable massive deployment of PV, electric mobility and electric heating," *Applied Energy*, vol. 287, p. 116 504, Apr. 1, 2021, ISSN: 0306-2619. DOI: 10.1016/j.apenergy.2021.116504. [Online]. Available: https://www.sciencedirect.com/science/article/pii/S0306261921000623 (visited on 01/19/2022).

[49] M. Resch, J. Bühler, B. Schachler, and A. Sumper, "Techno-Economic Assessment of Flexibility Options Versus Grid Expansion in Distribution Grids," *IEEE Transactions on Power Systems*, vol. 36, no. 5, pp. 3830–3839, Sep. 2021, ISSN: 1558-0679. DOI: 10.1109/TPWRS.2021.3055457.

[50] F. Scheller, R. Burkhardt, R. Schwarzeit, R. McKenna, and T. Bruckner, "Competition between simultaneous demand-side flexibility options: The case of community electricity storage systems," *Applied Energy*, vol. 269, p. 114 969, Jul. 1, 2020, ISSN: 0306-2619. DOI: 10.1016/j.apenergy.2020.114969. [Online]. Available: https://www.sciencedirect.com/science/article/pii/S0306261920304815 (visited on 01/19/2022).

[51] A. Rinaldi, S. Yilmaz, M. K. Patel, and D. Parra, "What adds more flexibility? An energy system analysis of storage, demand-side response, heating electrification, and distribution reinforcement," *Renewable and Sustainable Energy Reviews*, vol. 167, p. 112 696, 2022, ISSN: 1364-0321. DOI: 10.1016/j.rser.2022.112696. [Online]. Available: https://www.sciencedirect.com/science/article/pii/S1364032122005858.

[52] R. Sinha, B. Bak-Jensen, and J. R. Pillai, "Operational flexibility of electrified transport and thermal units in distribution grid," *International Journal of Electrical Power & Energy Systems*, vol. 121, p. 106 029, Oct. 1, 2020, ISSN: 0142-0615. DOI: 10.1016/j.ijepes.2020.106029. [Online]. Available: https://www.sciencedirect.com/science/article/pii/S014206151932633X (visited on 01/19/2022).

[53] A. Heider, L. Kundert, B. Schachler, and G. Hug, "Grid Reinforcement Costs with Increasing Penetrations of Distributed Energy Resources [unpublished]," *IEEE PowerTech2023*, 2023.

[54] E. Veldman and R. A. Verzijlbergh, "Distribution Grid Impacts of Smart Electric Vehicle Charging From Different Perspectives," *IEEE Transactions on Smart Grid*, vol. 6, no. 1, pp. 333–342, Jan. 2015, ISSN: 1949-3061. DOI: 10.1109/TSG.2014.2355494.

[55] A. Saavedra, M. Negrete-Pincetic, R. Rodríguez, M. Salgado, and Á. Lorca, "Flexible load management using flexibility bands," *Applied Energy*, vol. 317, p. 119 077, Jul. 1, 2022, ISSN: 0306-2619. DOI: 10.1016/j.apenergy.2022.119077. [Online]. Available: https://www.sciencedirect.com/science/article/pii/S0306261922004664 (visited on 04/04/2023).

[56] S. Stinner, K. Huchtemann, and D. Müller, "Quantifying the operational flexibility of building energy systems with thermal energy storages," *Applied Energy*, vol. 181, pp. 140–154, Nov. 1, 2016, ISSN: 0306-2619. DOI: 10.1016/j.apenergy.2016.08.055. [Online]. Available: https://www.sciencedirect.com/science/article/pii/S0306261916311424 (visited on 04/05/2023).

[57] J. Amme, G. Pleßmann, J. Bühler, L. Hülk, E. Kötter, and P. Schwägerl, *Distribution grid data generated by DINGO*, Zenodo, Apr. 7, 2017. DOI: 10.5281/zenodo.890479. [Online]. Available: https://zenodo.org/record/890479 (visited on 03/03/2023).

[58] L. Hülk, L. Wienholt, I. Cußmann, U. P. Müller, C. Matke, and E. Kötter, "Allocation of annual electricity consumption and power generation capacities across multiple voltage levels in a high spatial resolution," *International Journal of Sustainable Energy Planning and Management*, vol. 13, pp. 79–92, Sep. 28, 2017, ISSN: 2246-2929. DOI: 10.5278/ijsepm.2017.13.6. [Online]. Available: https://journals.aau.dk/index.php/sepm/article/view/1833 (visited on 03/03/2023).

[59] B. Schachler, A. Heider, T. Röpke, F. Reinke, and C. Bakker, "Assessing the impacts of market-oriented electric vehicle charging on german distribution grids," pp. 128–136, Jan. 1, 2021. DOI: 10.1049/icp.2021.2515. [Online]. Available: https://digital-library.theiet.org/content/conferences/10.1049/icp.2021.2515 (visited on 09/30/2022).

[60] A. Heider, K. Helfenbein, B. Schachler, T. Ropcke, and G. Hug, "On the Integration of Electric Vehicles into German Distribution Grids through Smart Charging," in *2022 International Conference on Smart Energy Systems and Technologies (SEST)*, Eindhoven, Netherlands: IEEE, Sep. 5, 2022, pp. 1–6, ISBN: 978-1-66540-557-7. DOI: 10.1109/SEST53650.2022.9898464. [Online].

Available: https://ieeexplore.ieee.org/document/9898464/ (visited on 11/18/2022).

[61] "Open_eGo," open_eGo, Open Electricity Grid Optimization. (), [Online]. Available: https://openegoproject.wordpress.com/ (visited on 03/24/2023).

[62] U. P. Müller, B. Schachler, and W.-D. Bunke, "Netzebenenübergreifendes Planungsinstrument zur Bestimmung des optimalen Netz- und Speicherausbaus in Deutschland integriert in einer OpenEnergyPlatform," Feb. 2019. [Online]. Available: https://www.uni-flensburg.de/fileadmin/content/abteilungen/industrial/dokumente/downloads/veroeffentlichungen/forschungsergebnisse/20190426endbericht-openego-fkz0325881-final.pdf (visited on 03/04/2023).

[63] "Demandlib - documentation." (), [Online]. Available: https://demandlib.readthedocs.io/en/latest/index.html (visited on 03/24/2023).

[64] "Open Energy Platform." (), [Online]. Available: https://openenergy-platform.org/ (visited on 03/04/2023).

[65] BNetzA, "Bestätigung Netzentwicklungsplan 2021-2035," Jan. 2022. [Online]. Available: https://data.netzausbau.de/2035-2021/NEP2035_Bestaetigung.pdf.

[66] K.-B. (KBA). "Bestand an Kraftfahrzeugen und Kraftfahrzeuganhängern nach Zulassungsbezirken." (2020), [Online]. Available: https://www.kba.de/DE/Statistik/Produktkatalog/produkte/Fahrzeuge/fz1_b_uebersicht.html?nn=3514348 (visited on 03/06/2023).

[67] B. f. V. u. d. I. BMDVI, *Mobilität in Deutschland 2017 / Zeitreihendatensatz*, Kelpin, Rene, Feb. 2019. [Online]. Available: http://www.mobilitaet-in-deutschland.de (visited on 03/05/2023).

[68] K. Helfenbein, "Analyse des Einflusses netzdienlicher Ladestrategien auf Verteilnetze aufgrund der zunehmenden Netzintegration von Elektrofahrzeugen," Hochschule für Technik und Wirtschaft Berlin, HTW, Berlin, Apr. 25, 2021.

[69] Destatis, "Gebäude und Wohnungen - Bestand an Wohnungen und Wohngebäuden - Bauabgang von Wohnungen und Wohngebäuden - Lange Reihen ab 1969 - 2021," Jul. 28, 2022. [Online]. Available: https://www.destatis.de/DE/Themen/Gesellschaft-Umwelt/Wohnen/Publikationen/Downloads-Wohnen/fortschreibung-wohnungsbestand-pdf-5312301.pdf?__blob=publicationFile.

[70] eGon development team, *eGon-data*, openego, Mar. 12, 2023. [Online]. Available: https://github.com/openego/eGon-data (visited on 04/04/2023).

[71] C. Büttner, J. Amme, J. Endres, A. Malla, B. Schachler, and I. Cußmann, "Open modeling of electricity and heat demand curves for all residential buildings

in Germany," *Energy Informatics*, vol. 5, no. 1, p. 21, Sep. 7, 2022, ISSN: 2520-8942. DOI: 10.1186/s42162-022-00201-y. [Online]. Available: https://doi.org/10.1186/s42162-022-00201-y (visited on 03/09/2023).

[72] "Dena-GEBÄUDEREPORT: Statistiken und Analysen zur Energieeffizienz im Gebäudebestand," 2016. [Online]. Available: https://www.dena.de/fileadmin/user_upload/8162_dena-Gebaeudereport.pdf (visited on 03/16/2023).

[73] "Pyomo," Pyomo. (), [Online]. Available: http://www.pyomo.org (visited on 04/03/2023).

[74] "Gurobi optimization," Gurobi Optimization. (), [Online]. Available: https://www.gurobi.com/ (visited on 04/03/2023).

[75] DIN e.V., "Merkmale der Spannung in öffentlichen Elektrizitätsversorgungsnetzen, DIN EN 50160:2020-11," pat., Nov. 2020. [Online]. Available: https://dx.doi.org/10.31030/3187943 (visited on 02/26/2023).

[76] elia group, "Aligning EV driver comfort with the needs of the power system in a new energy value chain. Accelerating to net-zero: Redefining energy and mobility," 2020.

[77] F. Toro, E. Jochem, O. Lösch, and M. Cerda, "Bewertung der Thermischen Energiespeicher (Latentwärmespeicher) als eine Option für industrieller Abwärmenutzung FuE-Bedarf, Hemmnisse und Empfehlungen - ein Statuspapier -," IREES, Karlsruhe, 2020.

[78] 5. T. GmbH, A. GmbH, T. T. GmbH, and T. GmbH, *Szenariorahmen zum Netzentwicklungsplan Strom 2035, Version 2021 Entwurf der Übertragungsnetzbetreiber*, Jan. 2020.